

Elsevier Editorial System(tm) for Palaeogeography, Palaeoclimatology, Palaeoecology

Manuscript Draft

Manuscript Number:

Title: Milankovitch-Timed Depositional Cyclicity Across the Lower Cretaceous Carbonate Platform, NE Mexico

Article Type: Research Paper

Section/Category:

Keywords: rock magnetics; Milankovitch theory; carbonates; anhysteretic remanent magnetization; paleoclimate

Corresponding Author: Dr. Diana K. Latta, PhD

Corresponding Author's Institution: Lehigh University

First Author: Diana K. Latta, PhD

Order of Authors: Diana K. Latta, PhD; David Anastasio, PhD; Maya Elrick, PhD; Kenneth P Kodama, PhD; Linda A Hinnov, PhD

Manuscript Region of Origin:

Abstract: Variations in rock magnetic parameters provide an objective tool, independent of facies, to correlate between proximal and distal Lower Cretaceous platform carbonates in northeast Mexico. Anhysteretic remanent magnetization (ARM), a rapid and non-destructive measurement is used for sub-meter scale stratigraphic correlation between inner and middle shelf deposits. Spectral analysis of variations in magnetic mineral concentrations within deposits from the upper Cupido Formation and basinal equivalent San Angel Limestone reveal periodicities consistent with Milankovitch orbital modes. Fluctuations in ferrimagnetic mineral concentrations are consistent with 405-, 123.9-, 94.9-, 51.2-, 39.4-, 22.5-, and 18.6-kyr orbital periodicities. Variations in ARM might reflect detrital (e.g. riverine, aeolian) or

diagenetic (e.g. chemical or thermal remagnetization, microbial mediated sulfate precipitation, bacterial magnetosomes) fluctuations in ferrimagnetic grain content. Rock magnetic and SEM/EDX analyses indicate that the ferrimagnetic grains are primary magnetite with grain sizes and shapes consistent with that of far-traveled dust. Variations in the magnetite grain abundance likely reflect regional changes in wind intensity and direction. In addition to the fine-grained magnetite population, inner shelf deposits record a periodic coarser-grained ferrimagnetic detrital mineral population interpreted to be an orbitally-driven watershed signal such as runoff variation. Time-series analysis of ARM data indicates similar accumulation rates for the inner and middle shelf deposits (8 cm/kyr) suggesting uniform thermal subsidence of the platform. Slower accumulation rates (7 cm/kyr) from outer shelf deposits suggest a limitation of the transport of material offshore.

1 **Milankovitch-Timed Depositional Cyclicality across the Lower**

2 **Cretaceous carbonate platform, NE Mexico**

3 **Diana K. Latta**

4 diana\_latta@lehigh.edu

5 Department of Earth and Environmental Sciences, Lehigh University, Bethlehem,

6 Pennsylvania 18015, USA

7 Phone: 610-758-3660

8 Fax: 610-758-3677

9

10 **David J. Anastasio**

11 dja2@lehigh.edu

12 Department of Earth and Environmental Sciences, Lehigh University, Bethlehem,

13 Pennsylvania 18015, USA

14 phone: 610-758-5117

15

16 **Maya Elrick**

17 dolomite@unm.edu

18 Department of Earth and Planetary Sciences, University of New Mexico, Albuquerque,

19 New Mexico 87131, USA

20 505-277-5077

21

22 **Kenneth P. Kodama**

23 kpk0@lehigh.edu

24 Department of Earth and Environmental Sciences, Lehigh University, Bethlehem,  
25 Pennsylvania 18015, USA  
26 phone: 610-758-3663

27

28 **Linda A. Hinnov**

29 hinnov@jhu.edu

30 Department of Earth and Planetary Sciences, Johns Hopkins University, Baltimore,  
31 Maryland 21218, USA  
32 phone: 410-516-5480

33

34 **ABSTRACT**

35 Variations in rock magnetic parameters provide an objective tool, independent of  
36 facies, to correlate between proximal and distal Lower Cretaceous platform carbonates in  
37 northeast Mexico. Anhysteretic remanent magnetization (ARM), a rapid and non-  
38 destructive measurement is used for sub-meter scale stratigraphic correlation between  
39 inner and middle shelf deposits. Spectral analysis of variations in magnetic mineral  
40 concentrations within deposits from the upper Cupido Formation and basinal equivalent  
41 San Angel Limestone reveal periodicities consistent with Milankovitch orbital modes.  
42 Fluctuations in ferrimagnetic mineral concentrations are consistent with 405-, 123.9-,  
43 94.9-, 51.2-, 39.4-, 22.5-, and 18.6-kyr orbital periodicities. Variations in ARM might  
44 reflect detrital (e.g. riverine, aeolian) or diagenetic (e.g. chemical or thermal  
45 remagnetization, microbial mediated sulfate precipitation, bacterial magnetosomes)  
46 fluctuations in ferrimagnetic grain content. Rock magnetic and SEM/EDX analyses

47 indicate that the ferrimagnetic grains are primary magnetite with grain sizes and shapes  
48 consistent with that of far-traveled dust. Variations in the magnetite grain abundance  
49 likely reflect regional changes in wind intensity and direction. In addition to the fine-  
50 grained magnetite population, inner shelf deposits record a periodic coarser-grained  
51 ferrimagnetic detrital mineral population interpreted to be an orbitally-driven watershed  
52 signal such as runoff variation. Time-series analysis of ARM data indicates similar  
53 accumulation rates for the inner and middle shelf deposits (8 cm/kyr) suggesting uniform  
54 thermal subsidence of the platform. Slower accumulation rates (7 cm/kyr) from outer  
55 shelf deposits suggest a limitation of the transport of material offshore.

56

57 **KEYWORDS:** rock magnetics, Milankovitch theory, carbonates, anhysteretic remanent  
58 magnetization, paleoclimate

59

## 60 **INTRODUCTION**

61 Meter-scale, upward-shallowing cycles are a common feature of many shallow-  
62 marine carbonate deposits throughout the stratigraphic record. The cycles, which are  
63 typically identified by lithologic (grain type and size, sedimentary structures, etc.) and  
64 biologic (fossil type, abundance, condition) characteristics, suggest repetitive changes in  
65 water depth as well as subaerial exposure. The changes in water depth have been  
66 attributed to orbitally-driven glacio-eustatic sea-level change (e.g. Fischer 1964,  
67 Grotzinger 1986, Goldhammer et al. 1987), tectonically driven changes in seafloor  
68 subsidence/uplift (e.g. Cisne 1986, Miall 1991), or internally driven changes in carbonate  
69 sediment production (e.g. Ginsburg 1971, Schlager 1981). Meter-scale cycles observed

70 in outer shelf, slope, and deep-sea deposits are also recognized by lithologic and biologic  
71 variations including changes in abundance of fine-grained carbonate, terrigenous, or  
72 siliceous material, organic matter, and/or bioturbation (e.g. Arthur et al. 1986, Einsele &  
73 Ricken 1991). Deep-water cycles do not record the direct effects of changing water  
74 depth because they accumulated at depths too great to cause sea-level induced facies  
75 change. Instead, they record paleoclimatic or paleoceanographic changes related to  
76 surface water productivity, dissolved oxygen content, and/or terrigenous influx (e.g. Dean  
77 & Arthur 1999). In either case, both shallow and deep water cycles are typically  
78 identified using lithologic and biologic criteria. Interpretations of both types of data are  
79 somewhat subjective and may be prone to error where units are thin, facies interpretations  
80 are ambiguous, or when facies transitions are subtle or non-existent. This subjectivity  
81 has been discussed and in some cases challenged and leads to weakness in  
82 cyclostratigraphic interpretations. In this paper, we provide a more objective tool to  
83 identify stratigraphic cyclicity within carbonate deposits and use this data to correlate  
84 between nearshore, offshore, and deep-sea successions at a resolution higher than typical  
85 biostratigraphy can provide, in some instances at the sub meter-scale.

86 Rock magnetic properties provides data, independent of facies or age, that allows  
87 for the impartial recognition of the presence or absence of cyclicity in carbonates,  
88 including those with frequencies equivalent to orbitally-driven climate cycles. Rock  
89 magnetic properties such as magnetic susceptibility (MS) have proven useful as  
90 paleoclimate indicators in a variety of depositional environments (e.g. Bloemendal et al.  
91 1995, Barthès et al. 1999, Ellwood et al. 2000, Kashiyama et al. 2003). MS is a sensitive  
92 recorder of the magnetic mineral concentration of a rock and can serve as a proxy for

93 high-frequency climate fluctuations in marine and lake sediments (Verosub & Roberts  
94 1995, Maher 1998, Kruiver et al. 1999, Ellwood et al. 2000, Kashiyama et al. 2003).  
95 Mayer and Appel (1999) have demonstrated that orbitally-driven cycles are recorded by  
96 MS variations in pelagic limestones of the Cretaceous Biancone Formation of the Italian  
97 Alps. In these deposits, the magnetic mineral is predominately ferrimagnetic magnetite  
98 and the MS is observed to vary inversely with carbonate content. Orbitally-driven cycles  
99 were also recorded by MS variations in Quaternary marine sediments from the equatorial  
100 Atlantic (Bloemendal et al. 1988). In these sediments, concentrations of magnetic  
101 minerals are controlled by aeolian dust from Africa, creating an MS chronology of  
102 climatic change across the Atlantic. Results from Tertiary sediments on the Ceara Rise in  
103 the equatorial Atlantic Ocean (ODP Leg 154) indicate MS data can vary on orbital time  
104 scales (Richter et al. 1997). Unfortunately, climatic interpretations from MS data are not  
105 unique, as MS in marine deposits varies inversely with carbonate content, and thus is  
106 very sensitive to changes in carbonate production and/or carbonate dissolution (e.g.  
107 Halfman et al. 1994, Barthès et al. 1999, Hoogakker et al. 2004, Mader et al. 2004).

108 An alternative way to use magnetic minerals to detect paleoclimate change within  
109 a stratigraphic succession, particularly one dominated by carbonate rocks, is to measure  
110 anhysteretic remanent magnetization (ARM). ARM is a measure of the concentration of  
111 ferrimagnetic minerals and is not sensitive to changes in carbonate content, and is thus an  
112 ideal tool for evaluating cycles independent of changing facies. Lean and McCave  
113 (1998) have demonstrated that glacial-interglacial variations are recorded by ARM  
114 variations in Pleistocene sediments on the Chatham Rise in the southwest Pacific Ocean  
115 (site 1123, core CHAT 1K). In these sediments the ARM is observed to increase during

116 interglacial periods in association with a decrease in productivity and an increase in the  
117 concentration of single-domain magnetite grains produced by magnetotactic bacteria.  
118 When used alone or in concert with MS, ARM is a powerful tool for objectively detecting  
119 cyclicity within carbonates, on a variety of time scales, including those associated with  
120 orbitally-driven cycles. The ability to use rock magnetic properties for identifying  
121 orbitally-driven climate cycles is especially significant within outer shelf and slope  
122 deposits which accumulate in water depths too great to record the lithologic effects of  
123 sea-level change and can result in the deposition of lithologically homogenous (non-  
124 cyclic) deposits. Results from Quaternary marine sediments from the north Atlantic  
125 Ocean (core SU921-18) show ARM data can vary on orbital time scales (Kruiver et al.  
126 1999). In these sediments, ARM and MS are perfectly correlated indicating  
127 ferrimagnetic minerals dominate the magnetic signal, which is not always true for  
128 carbonate-dominated rocks. Recognition of climatically-driven magnetic mineral  
129 variations in deep-water deposits and correlation of these records to coeval shelf strata,  
130 provides a high-resolution chronometer for assessing rates of sediment accumulation,  
131 sea-level rise and fall, isotopic excursions, extinction/radiation events, and biozone  
132 durations.

133         The objectives of this paper are to: 1) describe and interpret the causes of MS and  
134 ARM variability in coeval inner, middle and outer shelf carbonates in the Lower  
135 Cretaceous Cupido Formation and San Angel Limestone of northeastern Mexico, 2)  
136 demonstrate the occurrence of Milankovitch orbital periods defined by magnetic mineral  
137 variations, and 3) highlight the use of magnetic mineral variations in objectively defining

138 stratigraphic cyclicity and its use as a high-resolution chronometer in carbonate  
139 successions.

140

#### 141 **GEOLOGICAL SETTING and FORMATION DESCRIPTION**

142       Passive margin development along the Gulf Coast began in the Late Triassic  
143 following continental rifting in association with the opening of the Gulf of Mexico (e.g.  
144 Pindell 1993, Dickinson & Lawton 2001). Uplifted Paleozoic basement blocks and  
145 intervening grabens, played an important role in controlling Mesozoic depositional  
146 patterns along the Mexican Gulf Coast (e.g. Wilson 1990, Dickinson & Lawton 2001). In  
147 northeastern Mexico, the Coahuila block, presently bounded by the Sabinas and Parras  
148 Basins, served as a persistent basement high and a local source of clastic material, which  
149 influenced evaporite and subsequent carbonate deposition throughout northeastern and  
150 east-central Mexico (e.g. Wilson 1999).

151       By the earliest Cretaceous, extensive carbonate platforms developed around the  
152 entire Gulf of Mexico (e.g. Wilson 1999). In NE Mexico the shelf was shallow and  
153 rimmed with a stable grainstone shoal, represented by the Aptian Cupido and Albian  
154 Aurora Formations. The Cupido Formation (940 m thick) represents a distinct upward  
155 shoaling second-order megacycle, whose basinal equivalent is the Barremian to early  
156 Aptian San Angel Limestone. The Cupido Formation is conformable above the shales  
157 and limestones of the Barremian to early Aptian Taraises Formation (490 m thick) and  
158 conformably below the deeper-water shales and lime-mudstones of the La Peña  
159 Formation (~20-100 m thick). The Cupido Formation is characterized by stacked, meter-  
160 scale (1-8 m thick), upward-shallowing carbonate cycles composed of subtidal facies

161 overlain by intertidal to supratidal facies, which in some places are capped by subaerial  
162 exposure features (e.g. karst, paleosols, rubble breccias) (e.g. Goldhammer et al. 1991,  
163 Elrick 1995, Foster 2003).

164 In the Coahuila Marginal Folded Province of northeast Mexico the platform  
165 deposits of the Cupido Formation are exposed within strike-perpendicular canyons at the  
166 entrance to Potrero Garcia and Potrero Chico, a pair of conjoined evaporite-cored  
167 anticlines, that comprise the larger-scale, doubly-plunging, Sierra del Fraile anticlinorium  
168 (**Fig. 1a**). Here the Barremian through Albian successions are well-exposed and reveal  
169 the conformable contacts between the Cupido Formation and the underlying Taraises  
170 Formation and overlying deeper water La Peña Formation, which mark the drowning of  
171 the Cupido carbonate platform (e.g. Wall et al. 1961, Tinker 1982, Goldhammer et al.  
172 1991). The basinal equivalent San Angel Limestone is exposed in La Boca Canyon, a  
173 strike-perpendicular cross section through the Cerro de le Silla anticline (e.g. Longoria &  
174 Davila 1979, Longoria 1998) (**Fig. 1a**). Here the 684 m thick Barremian to early Aptian  
175 lime mudstones lie conformably above the massive-bedded limestones of the Barremian  
176 La Casita Formation and conformably below the Aptian La Peña Formation.

177 Our paleoclimatic study focuses on three Lower Cretaceous sections, each from a  
178 distinct position on the Cupido shelf: Garcia Canyon composed of peritidal-dominated  
179 inner shelf facies, Chico Canyon dominated by shallow subtidal middle shelf deposits,  
180 and La Boca Canyon composed of deep subtidal, outer shelf facies (San Angel  
181 Limestone) (**Fig. 1b**). The inner and middle shelf deposits were originally separated by  
182 ~25km, as determined by cross section restorations of Late Cretaceous Sevier-Laramide  
183 deformation. Inner shelf deposits are characterized by thin-bedded, peritidal and subtidal

184 facies, including evaporite, laminated mudstone, and burrowed packstone units. Middle  
185 shelf deposits contain similar peritidal and subtidal facies, but exhibit less frequent (less  
186 cyclic) facies changes, resulting in thicker-bedded units. Goldhammer et al. (1991)  
187 identified 78 upward-shallowing cycles within a ~270 m section in the inner shelf  
188 deposits at Garcia Canyon. Existing biostratigraphic control dated the section as 112 Ma  
189 to 110Ma. The authors interpreted the cycles (average thickness 3.44 m) to represent the  
190 40-kyr obliquity frequency (**Table 1**). More recent biostratigraphic constraints (e.g.  
191 Hardenbol et al. 1998) suggests the section represents ~3 Myrs, instead of 2 Myrs, further  
192 strengthening Goldhammer et al.'s (1991) lithologic-based assessment of orbitally-driven  
193 meter-scales cyclicity.

194         The inner and middle shelf deposits of the upper Cupido Formation at Garcia and  
195 Chico Canyons were chosen because of the presence of three regionally correlatable  
196 datums; the chronostratigraphically significant 120.0 Ma and 120.6 Ma sequence  
197 boundaries in the upper Cupido Formation and the relatively isochronous regionally  
198 transgressive basal La Peña Formation contact at ~117 Ma (e.g. Goldhammer 1999,  
199 Lehrmann et al. 1999) (**Fig. 1b**). Additionally, there are three 4th-order sequence  
200 boundaries identified between the 120.6 Ma and ~117 Ma datums, which can be  
201 stratigraphically correlated between the shelf locations, although with less certainty due  
202 to the lack of supratidal caps upsection in the middle shelf deposits. The lower La Peña  
203 Formation contact serves as the tie between the platform deposits and their equivalent  
204 outer shelf deposits of the San Angel Limestone. The correlative lithostratigraphic  
205 datums provide an opportunity to evaluate the genesis of magnetic variability in coeval

206 inner, middle, and outer shelf deposits in the Lower Cretaceous rocks of northeastern  
207 Mexico.

208         The regionally correlative datums represent sea-level lowstands at 120.59 Ma  
209 (AP2 of Hardenbol et al. 1998) and 120.0 Ma (AP3 of Hardenbol et al. 1998) and a sea-  
210 level highstand at 117.07 Ma (AP4 of Hardenbol et al. 1998). These 2nd-order sequence  
211 boundaries can be correlated to biostratigraphically-constrained sequence boundaries, in  
212 the northern Gulf of Mexico (e.g. Goldhammer 1999), within guyots in the Western  
213 Pacific (e.g. Röhl & Ogg 1998) and sedimentary basins of western Europe (e.g. Jacquin  
214 et al. 1998). These datums represent global changes in sea level during the Lower  
215 Cretaceous, a time when there was little or no global ice (e.g. Barron et al. 1984). During  
216 the Cretaceous greenhouse period, Jacobs and Sahagian (1993, 1995) argued that  
217 orbitally controlled changes in the sequestration of water on land could account for  
218 eustatic sea-level changes on the order of 2-8 m. In GCM models, Sloan and Huber  
219 (2001) demonstrated that precessional-driven changes in insolation could result in  
220 significant variability in the net surface ocean moisture balance and the amount of  
221 continental runoff at low latitudes during greenhouse conditions as in Cretaceous Mexico.

222

## 223 **SAMPLING STRATEGY**

224         Samples for rock magnetic studies were collected from the upper Cupido  
225 Formation at Garcia (inner shelf), Chico (middle shelf), and La Boca (outer shelf)  
226 canyons. The sampling resolution of between 20-50 cm was based on estimations of  
227 sedimentation rates using established chronostratigraphic datums for age control between

228 the regionally correlative 120.6 Ma sequence boundary (1.5 m thick collapse breccia) and  
229 the ~117 Ma La Peña Formation contact.

230 To potentially recover the precessional signal within the inner and middle shelf  
231 section we adjusted our sampling interval to every 20-50 cm in order to sample each  
232 facies change (**Fig. 2a,b**). Based on estimated accumulation rates of 14 cm/kyr in both  
233 the inner and middle shelf sections, we sampled every 1.4-3.5 kyrs. At the outer shelf  
234 section, we maintained a constant 30 cm (~4 kyr) sample spacing based on the calculated  
235 inner and middle shelf accumulation rate and on an average accumulation rate based on  
236 magnetostratigraphy for the San Angel Limestone and overlying La Peña Formation of  
237 ~3.2 cm/kyr (e.g. Clement et al. 2000) (**Fig. 2c**).

238 Individual, unoriented samples (297 inner shelf, 283 middle shelf, and 367 outer  
239 shelf) were collected and hand crushed to 2-4 mm size pieces and weighed in individual,  
240 pre-weighed, 8 cm<sup>3</sup> plastic sample boxes. Low-field bulk magnetic susceptibility (MS)  
241 was measured in order to determine the concentrations of all magnetic minerals on a  
242 Agico KLY-3s Kappabridge, while anhysteretic remanent magnetization (ARM), which  
243 measures the concentration of only the ferrimagnetic minerals, was acquired in a peak  
244 alternating fields from 100 mT to 0 mT with a DC field of 0.1 mT and measured on a 2G  
245 Enterprises, Inc. superconducting magnetometer. Both measurements were normalized  
246 for mass and measured at Lehigh University.

247 Variations in ARM can be due to fluctuations in primary ferrimagnetic mineral  
248 concentrations or diagenetic processes. In order to further characterize the magnetic grain  
249 size and composition, additional rock magnetic experiments were completed at the  
250 Institute for Rock Magnetism (IRM) of the University of Minnesota. Ferrimagnetic and

251 paramagnetic grains were characterized in 32 samples (11 inner shelf, 13 middle shelf,  
252 and 8 outer shelf) using the superconducting susceptometer (MPMS). After applying a  
253 2.5 T field, the magnetic moment of each sample was measured in a 0 T field at 5°K  
254 increments while heated from 20°K to 300°K. A 2.5 T field was then again applied at  
255 300°K and the magnetic moment of each sample was again measured in a 0 T field at 5°K  
256 increments while cooled back to 20°K. The relative populations of magnetic grains,  
257 based on variations in grain size of the ferrimagnetic and paramagnetic grains, were  
258 determined from 45 samples (16 inner shelf, 16 middle shelf, and 13 outer shelf) using  
259 the vibrating sample magnetometer (VSM1) where the field varied between 1.0 and -1.0  
260 T. In an additional experiment to determine the nature of the magnetic remanence,  
261 isothermal remanences (IRMs) were imparted to a single outer shelf sample (e.g. Lowrie  
262 1990) that displayed relatively high ferrimagnetic mineral concentrations and were  
263 subsequently thermally demagnetized (Latta et al. 2005). Finally, SEM/EDX images of  
264 magnetic grains collected from HCl-insoluble residues of samples that display hysteresis  
265 parameters characteristic of all shelf samples, were used to help elucidate ferrimagnetic  
266 grain morphology and size in order to further characterize the magnetic signal.

267

## 268 **ROCK MAGNETIC RESULTS**

269 The majority of MS values in each section are negative, with average MS values  
270 of  $-3.90 \times 10^{-8}$  m<sup>3</sup>/kg in the inner shelf deposits,  $-3.34 \times 10^{-9}$  m<sup>3</sup>/kg in the middle shelf  
271 deposits, and  $-2.93 \times 10^{-8}$  m<sup>3</sup>/kg in the outer shelf deposits (**Fig. 2**). These results are  
272 consistent with the abundance of diamagnetic (negatively susceptible) calcite in the  
273 carbonate rocks. Variations in the MS data series, resulting from variations in

274 concentrations of all magnetic minerals, do not show a consistent relationship between  
275 facies, at sequence boundaries, or within 5<sup>th</sup>-order upward-shallowing cycles (**Fig. 2**).  
276 Samples from different peritidal laminite intervals in the inner shelf deposits record both  
277 negative and positive MS values as is also true for different skeletal packstone intervals  
278 (**Fig. 2a**). At the AP3 (120.0 Ma) sequence boundary in the inner shelf section, MS is  
279 negative, whereas it is positive in the middle shelf deposits (**Figs. 2a,b**). In addition,  
280 while MS is positive at the AP2 sequence boundary in the middle shelf section it is  
281 negative at the AP3 sequence boundary (**Fig. 2b**).

282 Of particular interest, is that at our sampling resolution, there are no apparent  
283 correlations between meter-scale, upward-shallowing facies changes and MS or ARM  
284 values (**Fig. 2b inset**). For example, MS or ARM values do not systematically increase  
285 (or decrease) from subtidal cycle bases to intertidal/supratidal cycle caps in either the  
286 inner or middle shelf sections.

287 However, between inner and middle shelf sections, there is a good agreement with  
288 the stratigraphic position of discrete peaks of high MS values (e.g. 94.3, 124.0, and 133.0  
289 meters), but there is not an obvious correlation between the entire inner and middle shelf  
290 MS data series.

291 Average ARM values from each section range from  $4.03 \times 10^{-3}$  Am<sup>2</sup>/kg at the inner  
292 shelf,  $2.61 \times 10^{-3}$  Am<sup>2</sup>/kg at the middle shelf, and  $2.73 \times 10^{-3}$  Am<sup>2</sup>/kg at the outer shelf, and  
293 indicate the presence of ferrimagnetic minerals within the carbonates (**Fig. 2**). Similar to  
294 the MS data series, ARM values do not show a consistent relationship between facies, at  
295 sequence boundaries, or within 5<sup>th</sup>-order upward-shallowing cycles. However, unlike the  
296 MS data series, variations in the concentration of ferrimagnetic minerals between the

297 inner and middle shelf sections do exhibit a strong (68%) correlation (**Fig. 2a,b & 3a**).  
298 Stratigraphic intervals of high ARM values labeled 1 through 3 are separated by intervals  
299 of low ARM values (**Fig. 2a,b**). The MS and ARM trends at the middle shelf deposits  
300 mimic one another; however, this is not true at the inner and outer shelf deposits.  
301 Several individual peaks of higher ARM value labeled A through I can be correlated  
302 directly between the two shelf sections (**Fig. 2a,b & 3b**). This is particularly significant  
303 because these distinctive ARM peaks allow for correlation between the widely spaced  
304 stratigraphic sections at a sub-meter scale; a scale finer than that possible from  
305 biostratigraphy, facies-based cyclostratigraphy, or isotope stratigraphy.

306 Low-temperature magnetic measurements reveal a distinct transition around  
307 100°K, upon cooling from 300° to 20°K. The temperature of this sharp transition is  
308 consistent in all 11 inner shelf samples, 12 of the 13 middle shelf samples, and 7 of the 8  
309 outer shelf samples and is similar to that observed in the IRM Bestiary for magnetite  
310 w4000. The proximity of the magnetic transition to the Verwey transition (e.g.  
311 Muxworthy 1999) is suggestive of magnetite, however additional tests are needed to  
312 confirm the presence of the magnetite minerals (**Fig. 4**).

313 The ratio of saturation remanence magnetization to saturation magnetization  
314 (Mrs/Ms) versus magnetic coercivity (Hc), from all 45 samples measured using the  
315 vibrating sample magnetometer reveals that the majority of the magnetic minerals have  
316 pseudo single domain (PSD) size grains (0.1-10  $\mu\text{m}$ ) (Butler 1992) (**Fig. 5**). Seven  
317 samples had ratios consistent with single domain (SD) (<0.1  $\mu\text{m}$ ) or multi domain (MD)  
318 (>10  $\mu\text{m}$ ) size grains, but there is no pattern between depositional facies and magnetic  
319 grain size for these samples.

320 Magnetic hysteresis parameters for all 45 samples reveal a diamagnetic mineral  
321 component, shown to be calcite by x-ray diffraction. After removal of the diamagnetic  
322 contribution, hysteresis loops indicate the presence of a low-coercivity ferrimagnetic  
323 mineral population in all sections (**Fig. 6**). This is consistent with the identification of  
324 magnetite in the low-temperature magnetic results. In addition to this ferrimagnetic  
325 component, ‘wasp waisted’ hysteresis curves for some of the inner shelf samples indicate  
326 an additional population of high-coercivity ferrimagnetic minerals, which are noticeably  
327 absent from the middle and outer shelf samples (**Fig. 6a**).

328 IRM thermal demagnetization results indicate the presence of an intermediate (0.6  
329 T) coercivity ferrimagnetic mineral that has an unblocking temperature of 580°C, most  
330 likely magnetite, a small contribution from a high-coercivity (1.2 T) mineral, and a low-  
331 coercivity (0.1 T) minerals that has unblocking temperatures of 350°C suggestive of a  
332 sulfide mineral and 550°C indicating low-coercivity magnetite. IRM results failed to  
333 conclusively identify the composition of the high-coercivity mineral because of the small  
334 IRM, but since ARM measures only ferrimagnetic minerals that have coercivities below  
335 100 mT, the measurement is unable to detect this high-coercivity ferrimagnetic mineral  
336 population, and therefore those minerals do not affect our results. The IRM results (e.g.  
337 Lowrie 1990) indicate that the low-coercivity sulfide mineral contributes only 17% to the  
338 total IRM signal, while the intermediate- and low-coercivity magnetite mineral  
339 contributes the remaining 83%. Thus, IRM results support the assertion that  
340 ferrimagnetic magnetite minerals dominate the ARM data series. Furthermore, SIRM/ $\chi$   
341 ratios from four outer shelf samples indicate that the low-coercivity sulfide mineral is not  
342 greigite, a mineral common to marine deposits that could influence our ARM results. The

343 low-temperature experiments show this mineral is not siderite and it is unlikely that it is  
344 pyrrhotite.

345 SEM/EDX reveals numerous iron oxide grains ranging in size from 1.5 to 12  $\mu\text{m}$ ,  
346 where nearly 50% of the grains fall between 3.0 and 4.0  $\mu\text{m}$  (**Fig. 7**). SEM analyses  
347 further support the interpretation that the ferrimagnetic grains are detrital. The iron oxide  
348 grains are observed to have quartz coatings as expected from weathered bedrock and an  
349 absence of textures consistent with diagenetic processes. The grain shapes are not  
350 consistent with a biogenic origin (e.g. Bazylinski 1996).

351

## 352 **DISCUSSION OF ROCK MAGNETIC DATA**

353 The dominantly negative MS values support the obvious abundance of  
354 diamagnetic (negative susceptibility) calcite within the inner, middle and outer shelf  
355 deposits. MS records, which are less well-correlated to one another than ARM records,  
356 yet still retain a coherency in places of high and low magnetic variability, could represent  
357 a composite signal reflecting contributions from detrital (e.g. riverine or aeolian)  
358 magnetic grains and/or diagenetic (e.g. chemical or thermal remagnetization, microbial  
359 mediated sulfate precipitation, bacterial magnetosomes) magnetic minerals. ARM  
360 records from the widely separated inner and middle shelf sections display a strong (68%)  
361 suggesting that the variations in the ARM signal are not from a local or regional source  
362 (**Fig. 3**). In the middle shelf deposits, the high correspondence in the MS and ARM  
363 suggests that the ferrimagnetic minerals control the bulk magnetic behavior, while in the  
364 inner and outer shelf deposits, a lack of correlation between the MS and ARM records

365 suggests the ferrimagnetic mineral content within the rocks is a minor contribution to the  
366 bulk magnetic signature of those rocks.

367 It is significant that ARM records between the inner and middle shelf sections can  
368 be correlated, at both the ~15-20 m and sub-meter scales, using patterns in ARM values  
369 and discrete high ARM peaks (**Fig. 3a**). The synchronicity between the inner and middle  
370 shelf ARM data series and the lack of a similar high correlation in the MS data series is  
371 interesting, but not surprising. Within carbonate successions, if the ferrimagnetic mineral  
372 component is minor, the negatively susceptible calcite grains can dominate the bulk  
373 susceptibility, making identification of any positively susceptible paramagnetic or  
374 ferrimagnetic minerals, difficult. The successful correlation between inner and middle  
375 shelf sections using ARM records, and the inability to reach a similar successful  
376 correlation using MS records, highlights the utility of using ARM as an objective, high-  
377 resolution stratigraphic correlation tool in carbonate deposits. The ability to correlate  
378 widely spaced carbonate successions to one another, independent of facies, at the sub-  
379 meter scale is unparalleled by stratigraphic, biostratigraphic, magnetostratigraphic,  
380 isotopic, or typical down-hole geophysical techniques.

381 The lack of a relationship between patterns in magnetic values and patterns in  
382 facies, sequence boundaries, or within 5<sup>th</sup>-order upward-shallowing cycles is important to  
383 note. The observation that a particular carbonate facies (i.e. laminites, packstone, etc.)  
384 does not have a diagnostic magnetic signature, suggests that eustatic 5<sup>th</sup>-order sea-level  
385 changes controlling water depths do not control the input of fluvial or aeolian derived  
386 detrital magnetic minerals. Further, the observation that patterns in magnetic values do  
387 not correlate to facies patterns in upward-shallowing cycles driven by 5<sup>th</sup>-order sea-level

388 changes, also suggests that the relationship between orbitally-driven sea-level changes  
389 and changes in fluvial or wind-driven sedimentation patterns is non-linear. One might  
390 expect that when sea-level is low, magnetic values would increase with increasing fluvial  
391 influx as rivers respond to base line fall or increasing aeolian material with increasing  
392 windiness. Whereas when sea-level is high, one might expect magnetic values to  
393 decrease as accommodation increases and thus sediment accumulation and dilution by  
394 carbonates increases. Finally, the lack of a consistent magnetic signature at sequence  
395 boundaries, where strata are condensed and thus concentrations of magnetic minerals  
396 would be condensed is interesting. Possible variations in the amount of dissolution at  
397 each “condensed” interval could mask expected trend and lead to differences in measured  
398 magnetic values.

399         Hysteresis results support observations made from the MS and ARM data series  
400 in each section. Inner shelf deposits record 2 populations of ferrimagnetic minerals, a  
401 low-coercivity population, presumably magnetite as interpreted from low-temperature  
402 experiments, and a high-coercivity population, whose composition is undetermined. The  
403 presence of high-coercivity ferrimagnetic grains (only recorded by MS measurements  
404 since their coercivities are greater than 100 mT) could explain the lack of correlation  
405 between the MS and ARM records. Hysteresis results of middle shelf deposits indicate a  
406 single population of low-coercivity ferrimagnetic minerals. These results support our  
407 previous interpretation, based on the correlation between the MS and ARM records in  
408 these deposits, that magnetite plays an important role in controlling the bulk magnetic  
409 signature of the middle shelf rocks. Outer shelf deposits, like middle shelf deposits,  
410 record only one population of low-coercivity ferrimagnetic minerals, however this is

411 contrary to the observed lack of coherence between the MS and ARM records in these  
412 deposits. These results suggest that the concentration of magnetite is minor in the outer  
413 shelf deposits and that variations in diamagnetic or paramagnetic minerals play an  
414 important role in controlling the bulk magnetic character of these rocks. Low-  
415 temperature and hysteresis results agree with IRM results, supporting the validity that a  
416 ferrimagnetic magnetite mineral dominates our ARM data series.

417         The interpretation of a high-unblocking temperature magnetization carried by  
418 primary fine-grained magnetite agrees with Clement et al. (2000), for deposits in the  
419 nearby Sierra Madre Oriental fold belt. The characteristic remanent magnetization  
420 (ChRM) inclinations reported by Clement et al. (2000) are consistent with mid-  
421 Cretaceous inclinations predicted for those sites. Shallow synorogenic burial by during  
422 Late Cretaceous orogenesis was associated with peak temperatures of 150°C based on  
423 homogenization temperatures of fluid inclusions in the Cupido Formation at Garcia  
424 Canyon (Gray et al. 2001). Such temperatures can potentially lead to growth of new  
425 magnetic minerals and destruction of the primary magnetic grains; a possibility that we  
426 address by measuring IRMs during thermal demagnetization, SEM analysis of  
427 ferrimagnetic grain morphologies, and time-series analysis of the MS and ARM data  
428 series.

429         IRM results do indicate the presence of a low-coercivity sulfide mineral, however  
430 this mineral comprises only 17% of the total magnetic signal, with the remaining 83%  
431 controlled by intermediate- and low-coercivity magnetite. SEM/EDX analysis reveals  
432 that iron oxide shapes are inconsistent with those of diagenetic or biogenic grains, and  
433 more likely represent detrital grains, where the majority of the grain sizes are too small to

434 be derived from a strictly riverine source, and are instead consistent with that of far-  
435 traveled atmospheric dust (e.g. Chester et al. 1972, Pye 1987). Thus each rock magnetic  
436 and SEM analyses indicate that fine-grained detrital magnetite dominates the ARM signal  
437 in the inner, middle and outer shelf deposits, and that any secondary sulfide present is  
438 minor.

439

#### 440 **SPECTRAL ANALYSIS OF MAGNETIC DATA SERIES**

441 Lithologic and geochemical records of orbitally-driven cycles have been found in  
442 a variety of depositional environments and in rocks as old as the early Mesozoic (case  
443 studies in De Boer & Smith 1994, Shackleton et al. 1999, D'Argenio et al. 2004). While  
444 eccentricity frequencies are thought to have remained fairly constant since the  
445 Phanerozoic, the higher frequency obliquity and precession variations are thought to be  
446 sensitive to geodynamics, which can vary through time (e.g. Berger & Loutre 1994).  
447 Time-frequency analyses of the MS and ARM data series from each section were used to  
448 determine if variations in the magnetic data contained time frequencies consistent with  
449 previously reported Lower Cretaceous periodicities (i.e. 405-, 123.9-, 94.9-, 51.2-, 39.4-,  
450 22.5-, and 18.6-kyr; e.g. Park & Herbert 1987, Grippo et al. 2004). We use 'untuned'  
451 records of MS and ARM data as a function of stratigraphic position from the Lower  
452 Cretaceous sections to test for the presence of Milankovitch cycles and to evaluate  
453 climate encoding in lithologically cyclic, less cyclic and non-cyclic strata. Since  
454 diagenetic minerals are unlikely to contain periodicities consistent with Milankovitch  
455 orbital frequencies, spectral analysis of the magnetic data series also evaluates whether

456 remagnetization or new mineral growth during post-depositional burial was significant  
457 enough to destroy the primary magnetic minerals.

458         In the MS data, long-term variations in the series, representing any inadequately  
459 sampled low frequencies, were modeled using a 5<sup>th</sup> or 6<sup>th</sup>-order polynomial fit. The long-  
460 term variation was then removed from the MS data series and the ‘residual’ MS and raw  
461 ARM data were analyzed using the multitaper method (MTM) in the program  
462 Analyseries 1.2 (Paillard et al. 1996). The multitaper window was varied between  $2\pi$  and  
463  $3\pi$ , accommodating for both confidence and resolution of the output spectral estimators.  
464 A linear trend was estimated and removed and the data were normalized to unit variance.  
465 The magnetic data were then resampled at evenly spaced 0.1 m intervals and linearly  
466 interpolated. The resulting MS and ARM power spectra were then analyzed using a  
467 harmonic F-test to determine which sinusoidal components have a >90-95% significant  
468 contribution to the spectral power. It is important to note that “false positive” F-tests are  
469 possible. This occurs when the variance ratio, or the ratio of the power at the center of a  
470 spectral peak divided by the residual power (the center power subtracted from the  
471 average power across that peak) gets too high in cases when the residual power  
472 approaches zero. Such false positive F-tests tend to be associated with high frequencies  
473 where power is very low. Frequencies that exhibited high F-test values with very low to  
474 no power were disregarded.

475         The lowest frequency of the first significant peak in power on each spectral plot  
476 was assigned to the Cretaceous long eccentricity periodicity of 405-kyr (Laskar et al.  
477 2004, Table 6,  $g_2$ - $g_5$  term). The 405-kyr frequency is the lowest order Milankovitch  
478 frequency that our sampling strategy would have captured. Frequencies consistent with

479 longer orbital periodicities would have been inadequately sampled and subsequently  
480 removed by data preparation (i.e., polynomial fitting and removal). From the interpreted  
481 405-kyr frequency, the frequencies for remaining orbital rhythms [123.9, 94.9, 51.2, 39.4  
482 22.5 and 18.6-kyrs periodicities] were calculated and assigned to their appropriate  
483 stratigraphic frequency. Matches between calculated Milankovitch frequencies and  
484 spectral peaks were considered positive indicators that the magnetic data records cyclicity  
485 consistent with that particular orbital periodicity. Confirmation of cyclicity at predicted  
486 orbital frequencies supports the interpretation that the magnetic minerals are primary  
487 detrital grains whose abundance encodes climate variation. To further justify the  
488 assignment of the Milankovitch frequencies to the magnetic data series, spectrograms,  
489 comprised of moving-window unsmoothed periodgrams, were used to evaluate the  
490 stability of frequencies over time.

491

## 492 **RESULTS OF TIME-SERIES ANALYSIS**

493 Spectral results of MS and ARM data clearly indicate the presence of variations  
494 with frequencies predicted by Milankovitch theory in all three sections (**Table 1**). Power  
495 spectrum results of MS data from the inner, middle and outer shelf rocks reveal fewer  
496 orbital frequencies than ARM results, mainly because the majority of power is at low  
497 frequencies with relatively little power at higher frequencies, making positive  
498 identification of these Cretaceous orbital rhythms difficult. In the inner shelf deposits,  
499 the long eccentricity periodicity was assigned to the first peak in power at 0.038 cycles/m  
500 (28.6 m), and the remaining orbital rhythms, spaced according to known cycles ratios  
501 (e.g. Berger et al. 1989) (**Fig. 8a**). Inner shelf MS data series contain frequencies that

502 vary at the 128-kyr short eccentricity (8.2 m) and 51.2-kyr long obliquity (3.2 m)  
503 periodicities. An average accumulation rate of  $\sim 6.4$  cm/kyr for the inner shelf deposits,  
504 based on spectral analysis of the MS data, suggests the 135.4 m-thick datum-bounded  
505 measured at Garcia Canyon represents 2.23 Myrs.

506 Spectral analysis of MS data from the middle shelf deposits reveals peaks in  
507 power across the frequency spectrum. With assignment of the 405-kyr long eccentricity  
508 periodicity to the lowest significant frequency at 0.03 cycles/m (33.3 m), we are able to  
509 resolve significant peaks in power that correspond to frequencies consistent with the  
510 39.4-kyr short obliquity (3.2 m) and 22.5-kyr long precession index (1.8 m) periodicities  
511 (**Fig. 8b**). An average accumulation rate calculated for the middle shelf deposits at Chico  
512 Canyon is 8.0 cm/kyr, suggesting the 134.5 m-thick, datum-bounded measured section  
513 represents 1.79 Myrs.

514 Power spectra of the MS data from outer shelf deposits also reveal a dominance of  
515 power at low frequencies. With assignment of the first peak in power to the long  
516 eccentricity at 0.04 cycles/m (25 m), the remaining orbital rhythms are hard to identify  
517 (**Fig. 8c**). Although frequencies consistent with the 51.2- and 39.4-kyr long and short  
518 obliquity periodicities, respectively, are recognized by F-tests as statistically significant  
519 contributions to the data, lack of power at those particular frequencies suggests a ‘false  
520 positive’ F-test and thus those frequencies were ignored.

521 Unlike the MS power spectra, spectral results of the ARM data from all sections  
522 reveal power at all frequencies expected for Cretaceous orbital periodicities (**Table 1**). In  
523 the inner shelf rocks, the 405-kyr long eccentricity periodicity was assigned to the lowest  
524 significant frequency at 0.03 cycles/m (33.3 m) (**Fig. 9a**). Assignment of the remaining

525 orbital rhythms indicates that the ferrimagnetic data contain frequencies consistent with  
526 the 94.9-kyr short eccentricity (7.7 m), the 51.2- and 39.4-kyr long and short obliquity  
527 (4.2 m and 3.2 m), respectively, and the 22.5- and 18.6-kyr long and short precession  
528 index (1.8 m and 1.5 m) periodicities, respectively. Based on the spectral results of ARM  
529 data from the inner shelf deposits at Garcia Canyon, an average accumulation rate for the  
530 cyclic deposits is again 8.0 cm/kyr; suggesting the measured section represents 1.79  
531 Myrs.

532         Power spectra results of ARM data from middle shelf deposits also indicate  
533 significant power at discrete frequencies consistent with predicted Cretaceous orbital  
534 periodicities. With assignment of the 405-kyr long eccentricity periodicity to the 0.03  
535 cycles/m frequency (33.3 m), the 39.4-kyr short obliquity (3.2 m) and 22.5-kyr long  
536 precession index (1.8 m) periodicities also correspond to frequencies with peaks in power  
537 (**Fig. 9b**). The average accumulation rate based on power spectrum results of ARM data  
538 from the middle shelf deposits at Chico Canyon is 8.0 cm/kyr; suggesting the measured  
539 section represents 1.79 Myrs.

540         Power spectrum results of ARM data from the lithologically non-cyclic outer  
541 shelf deposits are significant and yield strong evidence for the encoding of Cretaceous  
542 orbital periodicities by ferrimagnetic minerals. With assignment of the 405-kyr long  
543 eccentricity period to the lowest significant peak in power at 0.035 cycles/m (28.6 m),  
544 calibration of the other spectral peaks indicates the positive identification of the 123-kyr  
545 short eccentricity (0.115 cycles/m), the 51.2 –kyr long and 39.4-kyr short obliquity  
546 (0.278 cycles/m and 0.370 cycles/m, respectively) and the 22.5-kyr long and 18.6-kyr  
547 short precession index band (0.625 cycles/m and 0.769 cycles/m, respectively) (**Fig. 9c**).

548 This interpretation results in an average sediment accumulation rate of 7 cm/kyr for the  
549 lime mudstones, suggesting that the 110 m measured section represents a duration of  
550 ~1.57 Myrs.

551 The outer shelf ARM spectrogram indicates the stability and constant strength of  
552 the eccentricity periodicities throughout most of the measured section with a shift to  
553 higher frequencies in the upper 20 m of the section. This shift could explain the power  
554 observed within the obliquity band and represent a decrease in accumulation rates. In  
555 addition, the analyses reveal an increase in strength and stability of the precession index  
556 in the upper 50 m of the section. The results highlight the ability of astronomically-tuned  
557 variations in magnetic minerals to detect changes in depositional processes, especially in  
558 lithologically homogeneous marine rocks.

559

## 560 **DISCUSSION**

561 Accumulation rates interpreted from power spectra of the ARM data series for the  
562 inner and middle shelf sections are virtually identical. Moving window power spectrum  
563 of the ARM data from the shelf deposits indicated consistent short-term accumulation  
564 rates of 8cm/kyr across each of the measured sections. Thus, long and short-term  
565 accumulation rates suggest uniform subsidence rates across the shelf for the ~1.79 Ma  
566 time window.

567 Even given the thickness similarity and the ability to lithologically correlate  
568 sequence boundaries as well as distinct intervals and discrete stratigraphic points using  
569 ARM records between the inner and middle shelf sections, it is surprising that these  
570 depositionally distinct successions record the same accumulation rate. This despite their

571 differences in facies distribution, degree of 5<sup>th</sup> order cycle development, and abundance  
572 of subaerial exposure horizons. The similarity in accumulation rates between the inner  
573 and middle shelf sections and agreement with accumulation rates (5-9 cm/kyr)  
574 determined from other carbonate platforms through time (e.g. Harms 1974, Rose 1976,  
575 Enos 1977), suggests that long-term thermal subsidence rates typical of passive-margins  
576 (1-25cm/kyr; Schlager 1981) plays a dominant role in controlling accumulation rates for  
577 these shallow-marine deposits during this 1.79 Myr time window.

578         Accumulation rates for the outer shelf deposits are less than rates for the inner and  
579 middle shelf sections, despite the fact that thermal subsidence rates along the outer shelf  
580 were likely the same or greater. This decrease may be the result of onshore-directed  
581 winds (**Fig. 10**) limiting offshore transport of shallow-shelf derived carbonates.

582         Characterization of the magnetite grains by rock magnetic and SEM/EDX  
583 analyses support ARM power spectrum results indicating that the primary magnetite  
584 minerals are detrital grains and not diagenetic or biogenic grains. Grain shapes are  
585 inconsistent with biogenic magnetosomes that are typically euhedral chains or diagenetic  
586 grains that have been grown *in situ* and thus would retain relatively unpitted grain surface  
587 morphologies. In addition, grain sizes for the majority of the primary detrital magnetite  
588 minerals are too small for a riverine source and are instead most characteristic of far-  
589 traveled aeolian dust (e.g. Chester et al 1972, Pye 1987). However, the coarser-grained  
590 ferrimagnetic mineral population observed only in the inner shelf deposits suggest that  
591 this nearshore environment records an influx of riverine detritus, most likely originating  
592 from the high-standing Coahuila block (e.g. Sloan & Huber 2001).

593           Prevailing wind directions and the proximity of the Mexican Cretaceous passive  
594 to an African aeolian source (e.g. Dean & Arthur 1999, Leuschner & Sirocko 2000)  
595 substantiates the conjecture that the ARM data records orbitally-driven changes in wind  
596 intensity and direction (**Fig. 10**). Dusts records from Lower Cretaceous marine deposits  
597 (DSDP cores 387, 391C, and 367) in the western Atlantic (e.g. Dean & Arthur 1999), and  
598 in modern Andean ice (e.g. Thompson et al. 1995), likewise are derived from African and  
599 record a paleoclimate signal.

600

## 601 **CONCLUSIONS**

602           Variations in rock magnetic properties provide an objective tool, independent of  
603 facies, to correlate between Lower Cretaceous carbonates in northeast Mexico. MS and  
604 ARM measurements are not controlled by facies, sequence boundaries, cyclicity patterns  
605 or carbonate production. ARM measurements, in particular, allow for stratigraphic  
606 correlations between inner and middle shelf deposits at the sub-meter scale. ARM is an  
607 underutilized tool for high-resolution stratigraphic correlations in carbonate deposits.

608           Rock magnetic experiments and SEM/EDX analysis of Lower Cretaceous  
609 carbonates indicate that ARM variations record variations in the concentrations of  
610 primary magnetite grains. Grain morphology and grain size distributions are consistent  
611 with that predicted for far-traveled atmospheric dust. Power-spectrum analysis of the  
612 MS and ARM magnetic data series from the inner, middle and outer shelf deposits,  
613 indicate variations in the concentrations of magnetic minerals consistent with Cretaceous  
614 Milankovitch frequencies of Berger et al. (1989). The positive identification of all  
615 Milankovitch orbital frequencies recorded by variations in ARM, further underscore that

616 the magnetite grains are primary detrital grains and not diagenetic or biogenic grains.  
617 The strong correlation in inner and middle shelf ARM records suggests a uniform source  
618 for the detrital magnetite grains. Changes in wind intensity or direction operating over  
619 precessional and longer orbital periodicities likely controlled the distribution of dust  
620 across the carbonate shelf. An observed coarser-grained detrital ferrimagnetic mineral  
621 population in the inner shelf deposits likely tracks precessionally-modulated runoff  
622 variability modulated by riverine deposition. The absence of this coarser-grained  
623 ferrimagnetic mineral population in the middle and outer shelf deposits suggests a local  
624 watershed in the Coahuila block and a limited ability to transport detritus to the middle or  
625 outer shelf.

626         Of particular interest is the observation that there is no consistent relationship  
627 between MS or ARM values and specific peritidal or subtidal facies or sequence  
628 boundary development. In addition, no obvious relationships between meter-scale  
629 upward-shallowing facies trends and magnetic mineral concentrations are observed  
630 suggesting a decoupling or non-linear relationship between orbitally controlled sea-level  
631 changes and orbitally controlled aeolian and/or fluvial influx.

632         Spectral results of the MS and ARM data series from the chronostratigraphic  
633 datum bounded inner and middle shelf sections indicate that accumulation rates across  
634 the platform were uniform. Consistent short- and long-term accumulation rates of 8  
635 cm/kyr for the depositionally distinct shelf sections, implies that long-term thermal  
636 subsidence rates, not variations in facies, carbonate production, or diagenesis, played the  
637 greater role in carbonate accumulation. Spectral results of ARM data for outer shelf

638 deposits suggest transport of material off the platform was limited, resulting in slower (7  
639 cm/kyr) accumulation rates.

640

#### 641 **ACKNOWLEDGMENTS**

642 We thank N.W. Harkins for field assistance and M. Jackson and P. Solheid for analytical  
643 assistance during DKL's fellowship at IRM. This study was supported by Collaborative  
644 National Science Foundation grant EAR-0230053 to Anastasio, Kodama, and Elrick, and  
645 graduate student research grants from the Geological Society of America, AAPG, and  
646 Sigma Xi to Latta. This paper represents a portion of DKL's Ph.D dissertation at Lehigh  
647 University.

648 **REFERENCES CITED**

649

650 Arthur, M.A., Bottjer, D.J., Dean, W.E., Fischer, A.G., Hattin, D.E., Kauffman, E.G.,  
651 Pratt, L.M., and Scholle, P.A., 1986, Rhythmic bedding in Upper Cretaceous  
652 pelagic carbonate sequences; varying sedimentary response to climate forcing:  
653 *Geology*, 4,153-156.

654

655 Barron, E.J., Hay, W.W., and Kauffman, E.G., 1984, Cretaceous climates: *Geology*,  
656 12, 21–47

657

658 Barthès, V., Pozzi, J.P., Vibert-Charbonnel, P, Thibal, J., and Mélières, M.A., 1999,  
659 High-resolution chronostratigraphy from downhole susceptibility logging tuned  
660 by paleoclimatic orbital frequencies: *Earth and Planetary Science Letters*, 165, 97-  
661 116.

662

663 Bazylinski, D.A., 1996, Controlled biomineralization of magnetic minerals by  
664 magnetotactic bacteria: *Chemical Geology*,132,191-198.

665

666 Berger, A., and Loutre, M.F., 1994, Astronomical forcing through geologic time, *in de*  
667 Boer, P.L., and Smith, D.G., eds., *Orbital forcing and cyclic sequences: Special*  
668 *Publication of the International Association of Sedimentologists*, 19,15-24.

669

670 Berger, A., Loutre, M.F., and Dehant, V., 1989, Milankovitch frequencies for pre-

671 Quaternary: Nature, 342, 133.  
672  
673 Bloemendal, J., King, W., Hunt, A., Demenocal, P.B., and Hayashida, A., 1995,  
674 Evidence for a change in the periodicity of tropical climate cycles at 2.4 Myr from  
675 whole-core magnetic susceptibility measurements: Nature, 342, 897-900.  
676  
677 Bloemendal, J., Lamb, B., and King, J., 1988, Paleoenvironmental implications of rock-  
678 magnetic properties of late Quaternary sediment cores from the eastern Equatorial  
679 Atlantic: Paleoceanography, 3, 61-87.  
680  
681 Butler, R.F., 1992, Paleomagnetism; magnetic domains to geologic terranes: Blackwell  
682 Scientific Publications, Boston, MA, 319 pp.  
683  
684 Chester, R., Elderfield, J.J., Griffin, J.J., Johnson, L.R., and Padgham, R.C., 1972, Eolian  
685 dust along the eastern margins of the Atlantic Ocean: Marine Geology, 13, 91-  
686 106.  
687  
688 Cisne, J., 1986, Earthquakes recorded stratigraphically in carbonate platforms: Nature,  
689 323, 320-322.  
690  
691 Clement, B.M., Poetisi, E., Bralower, T.J., CoBabe, E., and Longoria, J., 2000,  
692 magnetostratigraphy of mid-Cretaceous limestones from the Sierra Madre of  
693 northeastern Mexico: Geophysical Journal International, 143, 219-229.

694

695 D'Argenio, B., Fischer, A.G., Premoli-Silva, I., Weissert, H., and Ferreri, V., eds., 2004,  
696 Cyclostratigraphy: Approaches and Case Histories, SEPM Special Publication 81,  
697 311 pp.

698

699 Dean, W.E., and Arthur, M.A., 1999, Sensitivity of the North Atlantic Basin to cyclic  
700 climate forcing during the early Cretaceous: *Journal of Foraminiferal Research*,  
701 29, 465-486.

702

703 de Boer, P.L., and Smith, D.G., eds., 1994, Orbital forcing and cyclic sequences: Special  
704 Publication of the International Association of Sedimentologists 19, Blackwell  
705 Scientific Publications, Oxford, 559 pp.

706

707 Dickinson, W.R., and Lawton, T.F., 2001, Carboniferous to Cretaceous assembly and  
708 fragmentation of Mexico: *Geological Society of America Bulletin*, 113, 1142-  
709 1160.

710

711 Einsele, G., and Ricken, W., 1991, Limestone-marl alteration – an overview, *in* Einsele,  
712 G., Ricken, W., and Seilacher, A., eds., *Cycles and Events in Stratigraphy*,  
713 Springer, New York, pp. 23-47.

714

715 Ellwood, B.B., Crick, R.E., Hassani, A.E., Benoist, S.L., and Young, R.H., 2000,

716 Magnetosusceptibility event and cyclostratigraphy method applied to marine  
717 rocks: Detrital input versus carbonate productivity: *Geology*, 28, 1135-1138.  
718

719 Elrick, M., 1995, Cyclostratigraphy and sequence stratigraphy of the Lower Cretaceous  
720 Cupido Formation, northeastern Mexico: Annual Meeting Abstracts - American  
721 Association of Petroleum Geologists and Society of Economic Paleontologists  
722 and Mineralogists, 4, 26.  
723

724 Enos, P., 1977, Tamabra limestone of the Poza Rica trend, Cretaceous Mexico, *in* Cook,  
725 H.E., and Enos, P., eds., Deep-water carbonate environments: Society of  
726 Economic Paleontologists and Mineralogists, Special Publication 25, pp. 273-  
727 314.  
728

729 Fischer, A.G., 1964, The Lofer cyclothems of the Alpine Triassic, *in* Merriam, D.F., ed.,  
730 Symposium on Cyclic Sedimentation: Lawrence, KS, Kansas Geological Survey  
731 Bulletin 169, pp. 107-149.  
732

733 Foster, T.R., 2003, The evolution of a Lower Cretaceous carbonate platform within a  
734 divergent margin setting: The Cupido Formation, northeastern Mexico: M.S.  
735 Thesis, The University of Texas at Austin, Austin, Texas, 226 pp.  
736

737 Ginsburg, R.N., 1971, Landward movement of carbonate mud: new model for regressive

738 cycles in carbonates: American Association of Petroleum Geologists, 55,  
739 340.  
740  
741 Goldhammer, R.K., 1999, Mesozoic sequence stratigraphy and paleogeographic  
742 evolution of northeast Mexico, *in* Bartolini, C., Wilson, J.L., and Lawton, T.F.,  
743 eds., Mesozoic Sedimentary and Tectonic History of North-Central Mexico:  
744 Boulder, Colorado, Geological Society of America Special Paper 340, pp. 1-58.  
745  
746 Goldhammer, R.K., Dunn, P.A., and Hardie, L.A., 1987, High frequency glacio-eustatic  
747 sea-level oscillations with Milankovitch characteristics recorded in Middle  
748 Triassic platform carbonates in northern Italy: American Journal of Science, 287,  
749 853-892.  
750  
751 Goldhammer, R.K., Lehmann, P.J., Todd, R.G., Wilson, J.L., Ward, W.C., and Johnson,  
752 C.R., 1991, Sequence stratigraphy and cyclostratigraphy of the Mesozoic of the  
753 Sierra Madre Oriental, northeast Mexico, a field guidebook: Gulf Coast Section,  
754 Society of Economic Paleontologists and Mineralogists, 85 pp.  
755  
756 Gray, G.G., Pottorf, R.J., Yurewicz, D.A., Mahon, K.I., Pevear, D.R., and Chuchla, R.J.,  
757 2001, Thermal and Chronological Record of Syn- to Post-Laramide Burial and  
758 Exhumation, Sierra Madre Oriental, Mexico, *in* Bartolini, C, Buffler, R.T., and  
759 Cantú-Chapa, A, eds., The western Gulf of Mexico Basin: Tectonics, sedimentary  
760 basins, and petroleum systems: AAPG Memoir 75, pp. 159-181.

761  
762 Grippio, A., Fischer, A.G., Hinnov, L.A., Herbert, T.D., and Premoli Silva, I., 2004,  
763 Cyclostratigraphy and chronology of the Albian stage (Piobbico core, Italy), *in*  
764 D'Argenio, B., Fischer, A.G., Premoli-Silva, I., Weissert, H., and Ferreri, V., eds.,  
765 Cyclostratigraphy: Approaches and Case Histories, SEPM Special Publication  
766 No. 81, pp. 83-99.

767  
768 Grotzinger, J.P., 1986, Upward shallowing platform cycles: a response to 2.2 billion  
769 years of low-amplitude, high-frequency (Milankovitch band) sea level  
770 oscillations: *Paleoceanography*, 1, 403-416.

771  
772 Halfman, J.D., Johnson, T.C., and Finney, B.P., 1994, New AMS dates, stratigraphic  
773 correlations and decadal climatic cycles for the past 4 ka at Lake Turkana, Kenya:  
774 *Palaeogeography, Palaeoclimatology, Palaeoecology*, 111, 83-98.

775  
776 Hardenbol, J., Thierry, J., Farley, M.B., Jacquin, T., de Graciansky, P.-C., and Vail, P.R.,  
777 1998, Chart 4: Mesozoic and Cenozoic sequence chronostratigraphic framework  
778 of European basins: *in* de Graciansky, P.-C., Hardenbol, J., Jacquin, T., and Vail,  
779 P.R., eds., *Mesozoic and Cenozoic Sequence Stratigraphy of European Basins*,  
780 Society for Sedimentary Geology Special Publication 60, pp. 763-781.

781  
782 Harms, J.C., 1974, Brushy Canyon Formation, Texas: A deep-water density current  
783 deposit: *Geological Society of America Bulletin*, 85, 1763-1784.

784

785 Hoogakker, B.A.A., Rothwell, R.G., Rohling, E.J., Paterne, M., Stow, D.A.V., Herrle,  
786 J.O., and Clayton, T., 2004, Variations in terrigenous dilution in western  
787 Mediterranean Sea pelagic sediments in response to climate change during the last  
788 glacial cycle: *Marine Geology*, 211, 21-43.

789

790 Jacobs, D.K., and Sahagian, D.L., 1993, Climate-induced fluctuations in sea-level during  
791 non-glacial times: *Nature*, 361, 710-712.

792

793 Jacobs, D.K., and Sahagian, D.L., 1995, Milankovitch fluctuations in sea level and recent  
794 trends in sea-level change: Ice may not always be the answer: *in* Haq, B.U., ed.,  
795 Sequence Stratigraphy and Depositional Response to Eustatic, Tectonic and  
796 Climate Forcing, Kluwer Academic Press, Netherlands, pp. 329-366.

797

798 Jacquin, T., Rusciadelli, G., Amedro, F., de Graciansky, P.-C., and Magniez-Jannin, F.,  
799 1998, The North Atlantic cycle; an overview of 2nd-order transgressive/regressive  
800 facies cycles in the Lower Cretaceous of Western Europe: *in* de Graciansky, P.-  
801 C., Hardenbol, J., Jacquin, T., and Vail, P.R., eds., *Mesozoic and Cenozoic*  
802 *Sequence Stratigraphy of European Basins*, Society for Sedimentary Geology  
803 Special Publication 60, pp. 397-409.

804

805 Kashiyama, Y., Fastovsky, D.E., Rutherford, S., King, J., and Montellano, M., 2003,

806 Genesis of a locality of exceptional fossil preservation: paleoenvironments of  
807 Tepexi de Rodríguez (mid-Cretaceous, Puebla, Mexico): *Cretaceous Research*,  
808 24, 407-431.

809

810 Kruiver, P.P., Kok, Y.S., Dekkers, M.J., Langereis, C.G., and Laj, C., 1999, A pseudo-  
811 Thellier relative palaeointensity record, and rock magnetic and geochemical  
812 parameters in relation to climate during the last 276 kyr in the Azores region:  
813 *Geophysical Journal International*, 136, 757-770.

814

815 Laskar, J., Robutel, P., Joutel, F., Gastineau, M., Correia, A.C.M., and Levrard, B., 2004,  
816 A long-term numerical solution for the insolation quantities of the Earth,  
817 *Astronomy and Astrophysics*, 428, 261-285.

818

819 Lean, C.M.B., and McCave, I.N., 1998, Glacial to interglacial mineral magnetic and  
820 palaeoceanographic changes at Chatham Rise, SW Pacific Ocean: *Earth and*  
821 *Planetary Science Letters*, 163, 247-260.

822

823 Lehrmann, D.J., and Goldhammer, R.K., 1999, Secular variation in parasequence and  
824 facies stacking patterns of platform carbonates: A guide to application of  
825 stacking-patterns analysis in strata of diverse ages and settings, *in* Harris, P.M.,  
826 Saller, A.H., and Simo, J.A., eds., *Advances in carbonate sequence stratigraphy;*  
827 *application to reservoirs, outcrops and models: Special Publication - Society for*  
828 *Sedimentary Geology*, 63, pp.187-225.

829

830 Leuschner, D.C., and Sirocko, F., 2000, The low-latitude monsoon climate during  
831 Dansgaard-Oeschger cycles and Heinrich Events: *Quaternary Science Reviews*,  
832 19, 243-254.

833

834 Longoria, J.F., 1998, The Mesozoic of the Mexican Cordillera in Nuevo Leon, NE  
835 Mexico, *in* Longoria, J.F., Krutak, P.R., and Gamper, M.A., eds., *Geologic*  
836 *Studies in Nuevo Leon, Mexico: Sociedad Mexicana de Paleontologia, A.C.*  
837 *Special Publication*, pp. 1-44.

838

839 Longoria, J.F., and Davila, V.A., 1979, Estratigrafia y microfacies del Cerro de la Silla,  
840 SE de Monterrey, Nuevo Leon: *Boletin del Departamento de Geologia Uni-Son*,  
841 2, 64-95.

842

843 Lowrie, W. 1990, Identification of ferromagnetic minerals in a rock by coercivity and  
844 unblocking temperature properties: *Geophysical Research Letters*, 17, 159-162.

845

846 Mader, D., Cleaveland, L., Bice, D.M., Montanari, A., and Koeberl, C., 2004, High-  
847 resolution cyclostratigraphic analysis of multiple climate proxies from a short  
848 Langhian pelagic succession in the Conero Riviera, Ancona (Italy):  
849 *Palaeogeography, Palaeoclimatology, Palaeoecology*, 211, 325-344.

850

851 Maher, B.A., 1998, Magnetic properties of modern soils and Quaternary loessic

852 paleosols; paleoclimatic implications: *Palaeogeography, Palaeoclimatology,*  
853 *Palaeoecology*, 137, 25-54.

854

855 Mayer, H., and Appel, E., 1999, Milankovitch cyclicity and rock magnetic signatures of  
856 paleoclimate change in Early Cretaceous Biancone Formation of Southern Alps,  
857 Italy: *Cretaceous Research*, 20, 189-214.

858

859 Miall, A., 1991, Stratigraphic sequences and their chronostratigraphic correlation: *Journal*  
860 *of Sedimentary Petrology*, 61, 497-505.

861

862 Muxworthy, A.R., 1999, Low-temperature susceptibility and hysteresis of magnetite:  
863 *Earth and Planetary Science Letters*, 169, 51-58.

864

865 Paillard, D., Labeyrie, L., and Yiou, P., 1996, Macintosh program performs time-series  
866 analysis: *Eos Transactions American Geophysical Union*, 77, 379.

867

868 Park, J., and Herbert, T.D., 1987, Hunting for paleoclimatic periodicity in a geologic time  
869 series with an uncertain scale, *Journal of Geophysical Research*, 92, 14027-14040.

870

871 Pindell, J.L., 1993, Regional synopsis of Gulf of Mexico and Caribbean evolution, *in*  
872 Pindell, J.L., and Perkins, B.F., eds., *Mesozoic and Early Cenozoic Development*  
873 *of the Gulf of Mexico and Caribbean Region, A Context for Hydrocarbon*

874 Exploration: Gulf Coast SEPM Foundation 13<sup>th</sup> Annual Research Conference  
875 Proceedings, pp. 251-274.  
876  
877 Pye, K., 1987, *Aeolian Dust and Dust Deposits*: Academic Press, London, 334 pp.  
878  
879 Richter, C., Valet, J.-P., and Solheid, P.A., 1997, Rock magnetic properties of sediments  
880 from Ceara Rise (Site 929); implications for the origin of the magnetic  
881 susceptibility signal: *in* Shackleton, N.J., Curry, W.B., Richter, C., and Bralower,  
882 T.J., eds., *Proceedings of the Ocean Drilling Program, Scientific Results*, 154,  
883 pp.169-179.  
884  
885 Röhl, U., and Ogg, J.G., 1998, Aptian-Albian eustatic sea-levels: Special Publication of  
886 the International Association of Sedimentologists, 25, 95-136.  
887  
888 Rose, P., 1976, Mississippian carbonate shelf margins, western United States: U.S.  
889 Geological Survey Journal of Research, 4, 449-466.  
890  
891 Schlager, W., 1981, The paradox of drowned reefs and carbonate platforms: Geological  
892 Society of America Bulletin, 92:197–211.  
893  
894 Scotese, C.R., Gahagan, L.M., and Larson, R.L., 1989, Plate tectonic reconstructions of

895 the Cretaceous and Cenozoic ocean basins, *in* Scotese, C.R. and Sager, W.W.,  
896 (eds.), Mesozoic and Cenozoic plate reconstructions, Elsevier, Amsterdam, pp.  
897 27-48.

898

899 Shackleton, N.J., McCave, I.N., and Weedon, G.P., 1999, A Discussion: Astronomical  
900 (Milankovitch) Calibration of the Geological Timescale, Philosophical  
901 Transactions of the Royal Society, London, Series A, 357, 1733-2007.

902

903 Sloan, L.C., and Huber, M, 2001, Eocene Oceanic Response to Orbital Forcing on  
904 Precessional Time Scales: Paleoceanography, 16, 101-111.

905

906 Thompson, L.G., Mosley-Thompson, E., Davis, M.E., Lin, P.N., Henderson, K.A., Cole-  
907 Dai, J., Bolzan, J.F., and Liu, K. B., 1995, Late Glacial Stage and Holocene  
908 tropical ice core records from Huscaran, Peru: Science, 269, 46-50.

909

910 Tinker, S.W., 1982, Lithostratigraphy and biostratigraphy of the Aptian La Peña  
911 Formation, northeast Mexico and southeast Texas, and the depositional setting of  
912 the Aptian Pearsall-La Peña Formations, Texas subsurface and northeast Mexico:  
913 Why is there not another Fairway Field? [M.S. Thesis]: Ann Arbor, University of  
914 Michigan, 80 pp.

915

916 Verosub, K.L., and Roberts, A.P., 1995, Environmental magnetism: past, present, and  
917 future: Journal of Geophysical Research, 100, 2175-2192.

918

919 Wall, J.R., Murray, G.E., and Diaz, T., 1961, Geology of the Monterrey area, Nuevo  
920 Leon, Mexico: Transactions - Gulf Coast Association of Geological Societies, 11,  
921 57-71.

922

923 Wilson, J.L., 1990, Basement structural controls on Mesozoic carbonate facies in  
924 northeastern Mexico – a review: Special Publication of the International  
925 Association of Sedimentologists, 9, 235-255.

926

927 Wilson, J.L., 1999, Controls on the wandering path of the Cupido Reef trend in  
928 northeastern Mexico, *in* Bartolini, C., Wilson, J.L., and Lawton, T.F., eds.,  
929 Mesozoic Sedimentary and Tectonic History of North-Central Mexico: Boulder,  
930 Colorado, Geological Society of America Special Paper 340, pp. 135-143.

931

932

### 933 **FIGURE CAPTIONS**

934

935 **Figure 1a.** Index and hillshade maps locating the Lower Cretaceous inner (Garcia),  
936 middle (Chico), and outer (La Boca) shelf measured sections in the foreland of the Sierra  
937 Madre Oriental fold belt, northeast Mexico. **b.** Coeval inner and middle shelf deposits of  
938 the upper Cupido Formation and basinal equivalent outer shelf deposits of the San Angel.  
939 Regionally correlative datums (AP2-4 of Hardenbol et al. 1998) provide  
940 chronostratigraphic constraint. Pie charts illustrate facies distribution across the platform

941 and indicate inner shelf deposits are dominated by peritidal facies, middle shelf deposits  
942 are dominated by subtidal facies, while outer shelf deposits are characterized by a  
943 homogenous succession of basinal lime mudstones. Details of studied sections in **Figure**  
944 **2**.

945

946 **Figure 2.** MS and ARM variations compared to lithofacies for the inner, middle, and  
947 outer shelf measured sections. Chronostratigraphic datums AP2 (120.59 Ma), AP3 (120  
948 Ma), and AP4 (~117 Ma) based on measured sections from Foster 2004 and age  
949 constraint from Hardenbol et al. 1998. **a.** Inner shelf stratigraphy dominated by cyclic  
950 peritidal facies. **b.** Middle shelf stratigraphy dominated by weakly cyclic shallow  
951 subtidal facies. Inset figure shows lack of correlation between facies and magnetic  
952 variations. **c.** Outer shelf facies composed entirely of noncyclic bioturbated (hatched  
953 layers) dark lime mudstones. Peaks in ARM labeled A-I are correlated between the inner  
954 and middle shelf sections. Intervals of higher ARM values labeled 1-3 can also be  
955 correlated across the shelf sections.

956

957 **Figure 3a.** Comparison of ARM values between inner and middle shelf measured  
958 sections in the upper Cupido Formation. **b.** Detailed view of the upper 60 meters. Note  
959 the close correlation of ARM values at the sub-meter scale marked by peaks A-I.

960

961 **Figure 4.** Representative low-temperature magnetic measurements for inner, middle, and  
962 outer shelf deposits indicating a sharp transition (~100°K) upon cooling (black circles)  
963 suggesting the ARM signal is likely controlled by ferrimagnetic magnetite minerals (e.g.

964 Muxworthy 1999). This sharp decrease in room temperature IRM is similar to that  
965 observed for magnetite w4000 in the IRM Bestiary.

966

967 **Figure 5.** Modified Day plot highlighting the distribution of grain sizes of magnetic  
968 minerals from a subset of samples from inner (n=16), middle (n=16), and outer (n=13)  
969 shelf deposits. Most samples fall within PSD grain sizes between 0.1-10  $\mu\text{m}$ ,  
970 characteristic of grain sizes of far transported aeolian detritus.

971

972 **Figure 6.** Hysteresis curves of representative samples from each measured section, with  
973 the diamagnetic component removed. **a.** Inner shelf deposits exhibit two populations of  
974 magnetic minerals as shown by the wasp-waisted hysteresis curves; a low-coercivity  
975 ferrimagnetic mineral population and high-coercivity ferrimagnetic mineral population.  
976 **b.** Middle shelf deposits, and **c.** outer shelf deposits indicate the presence of a single low-  
977 coercivity ferrimagnetic mineral population.

978

979 **Figure 7.** Magnetite grain sizes analyzed from HCl-insoluble residues by SEM/EDX.  
980 Average grain size 3.3  $\mu\text{m}$  ( $\pm 1 \mu\text{m}$ ) is consistent with that of far-traveled atmospheric  
981 dust particles. Inset background electron image of an iron-oxide grains with quartz  
982 coatings, suggestive of original quartz cement and detrital origin of grains.

983

984 **Table 1.** Comparison of encoded Milankovitch frequencies using lithology, MS and  
985 ARM variations and the calculated average accumulation rates.

986

987 **Figure 8.** MTM spectral analysis of MS data series. Cretaceous frequencies consistent  
988 with predicted orbital periodicities are shown by arrows and labeled accordingly. Note  
989 the difficulty of resolving these periodicities when analyzing variations in all magnetic  
990 minerals. **a.** MS data from inner shelf deposits indicate power is dominated at low  
991 frequencies. **b.** MS data from middle shelf rocks mimic the associated ARM data, shown  
992 in **Figure 9**, and yield discrete peaks in power at corresponding predicted Cretaceous  
993 orbital frequencies. **c.** MS data from outer shelf deposits, like the inner shelf rocks,  
994 indicate power is dominated at low frequencies.

995

996 **Figure 9.** MTM spectral analysis of ARM data series (ferrimagnetic minerals). **a.** ARM  
997 data from inner shelf deposits yield discrete peaks in power at all predicted Cretaceous  
998 orbital frequencies. **b.** ARM data from middle shelf rocks mimic the associated MS data,  
999 shown in **Figure 8**, and yield discrete peaks in power at corresponding predicted  
1000 Cretaceous orbital frequencies. **c.** ARM data from outer shelf deposits, like the inner  
1001 shelf rocks, yield well-defined peaks in power at all predicted Cretaceous orbital  
1002 frequencies.

1003

1004 **Figure 10.** Paleogeographic reconstruction of the Atlantic Ocean during the middle  
1005 Cretaceous (*modified from Scotese et al. 1989*). Star denotes the location of the study  
1006 sites in northeast Mexico, dark grey indicates continent, light gray represents shallow  
1007 marine environments and double lines indicate the orientation of the mid-ocean ridge.  
1008 Arrows denote the likely wind directions suggesting transport of dust from Africa to the  
1009 study area.

Figure 1  
[Click here to download high resolution image](#)

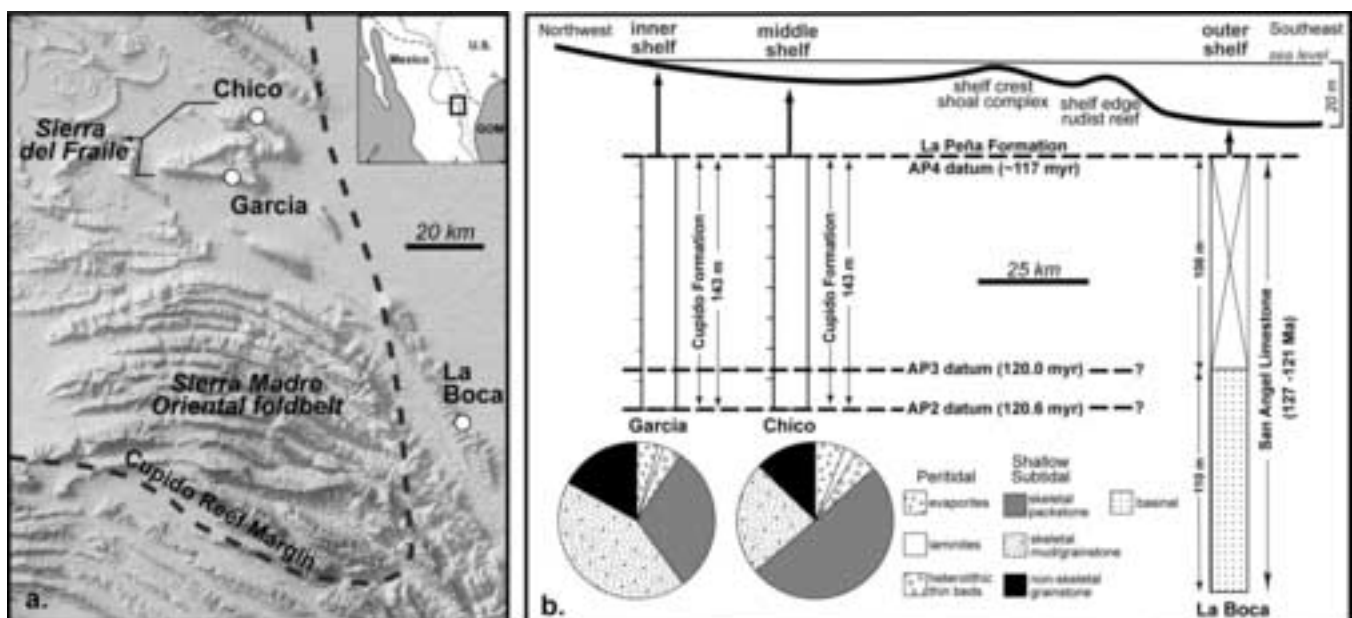


Figure 2a

[Click here to download high resolution image](#)

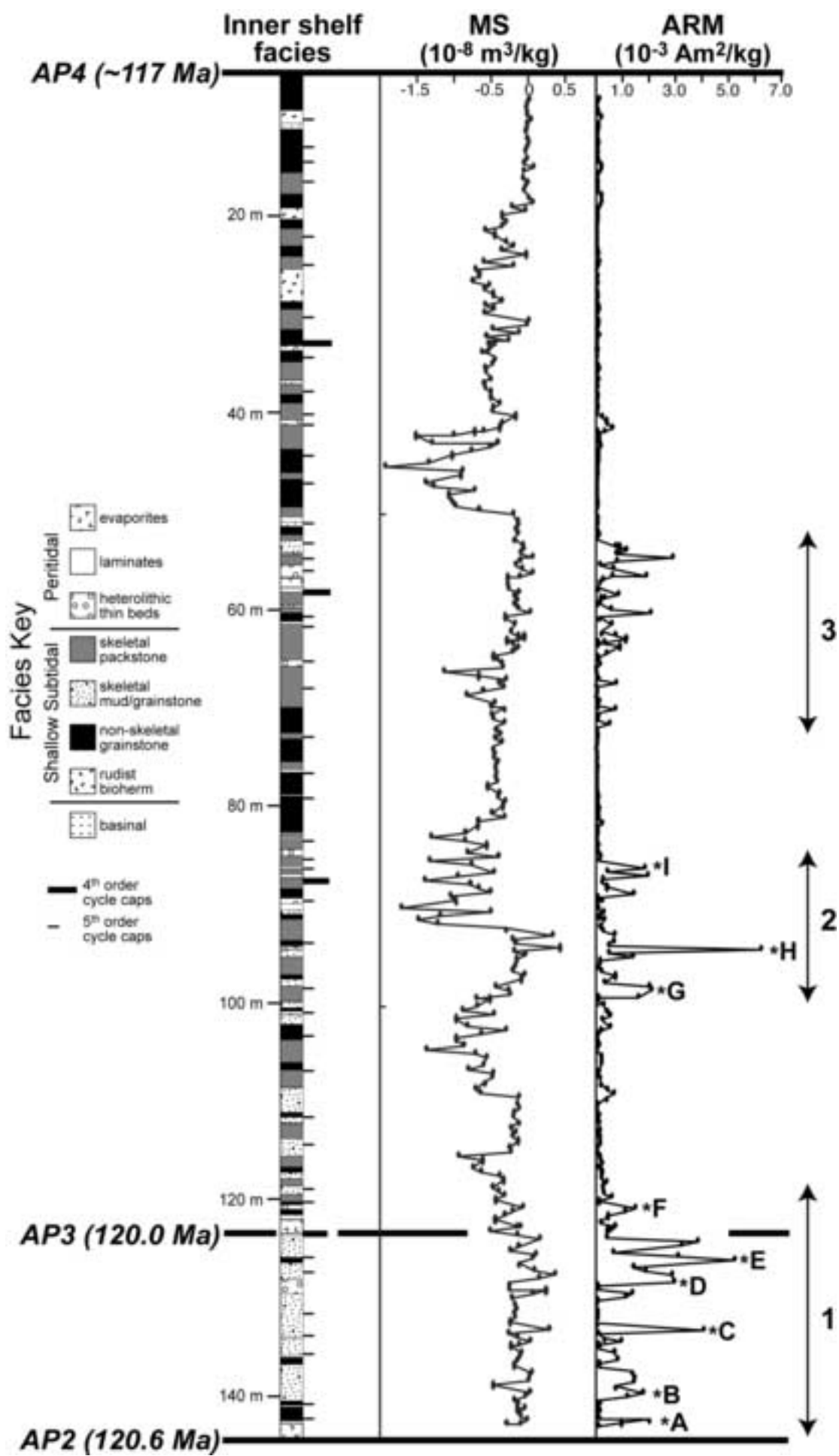


Figure 2b  
[Click here to download high resolution image](#)

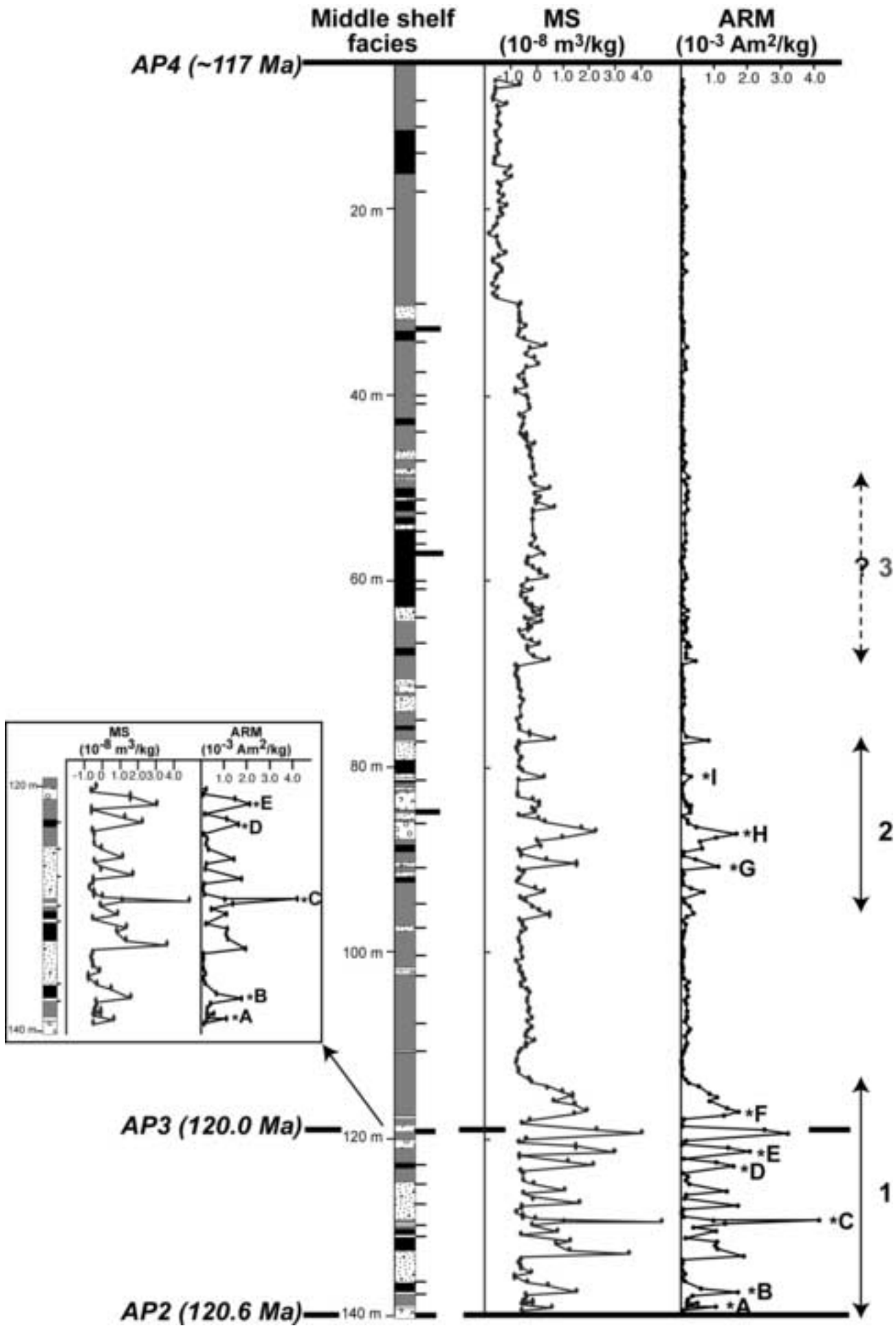


Figure 2c  
[Click here to download high resolution image](#)

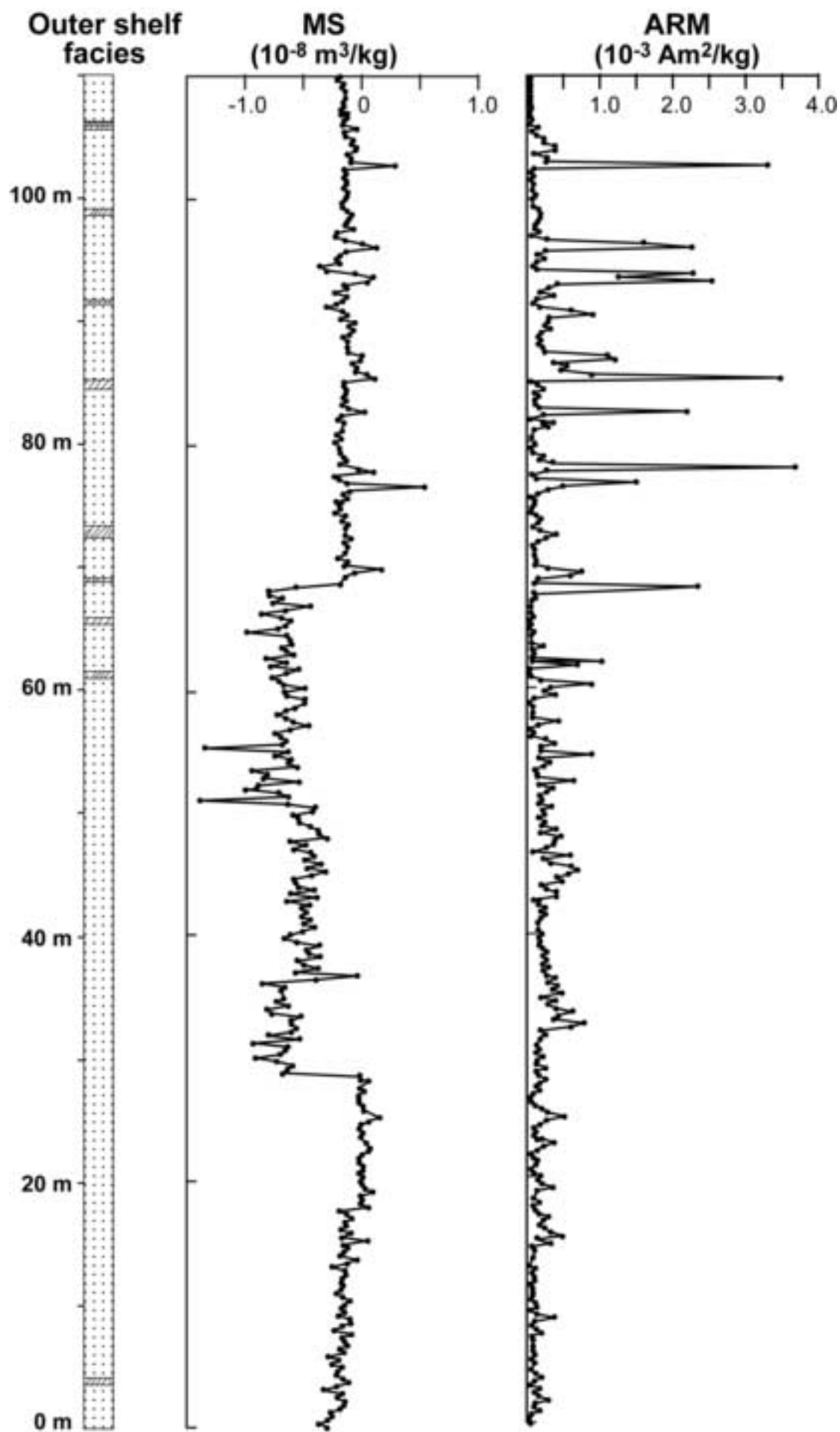


Figure 3

[Click here to download high resolution image](#)

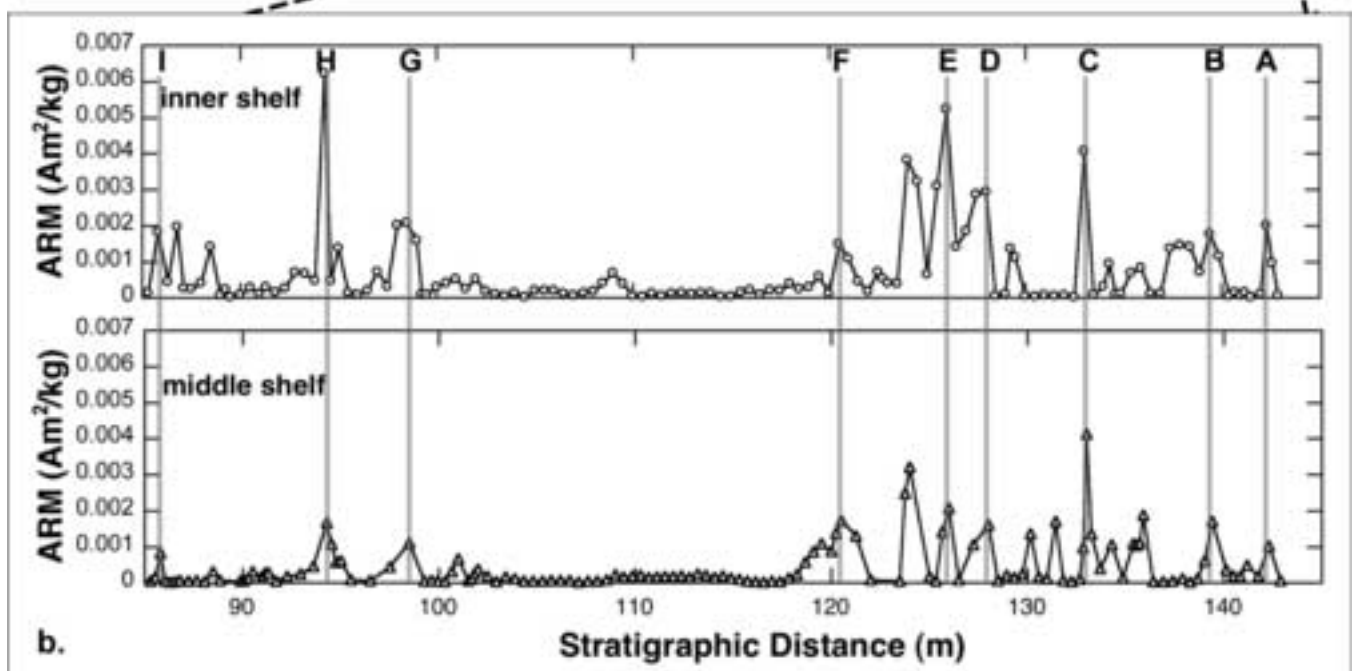
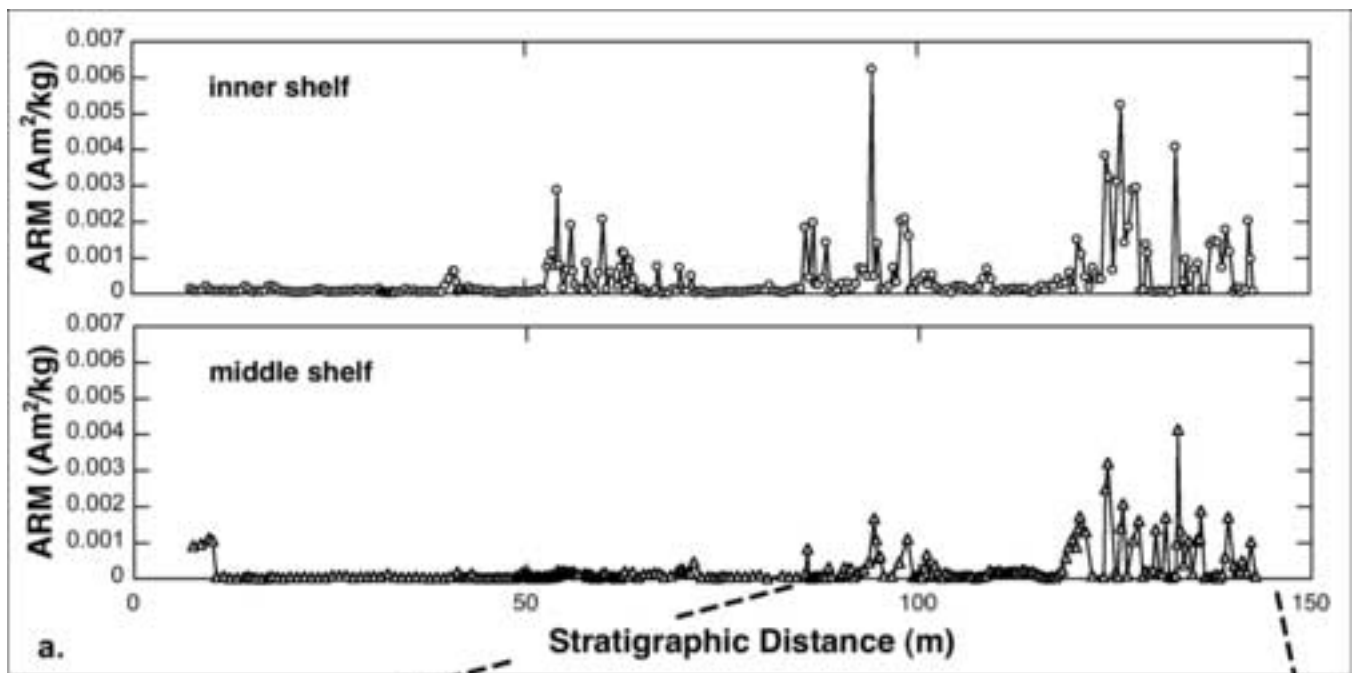


Figure 4  
[Click here to download high resolution image](#)

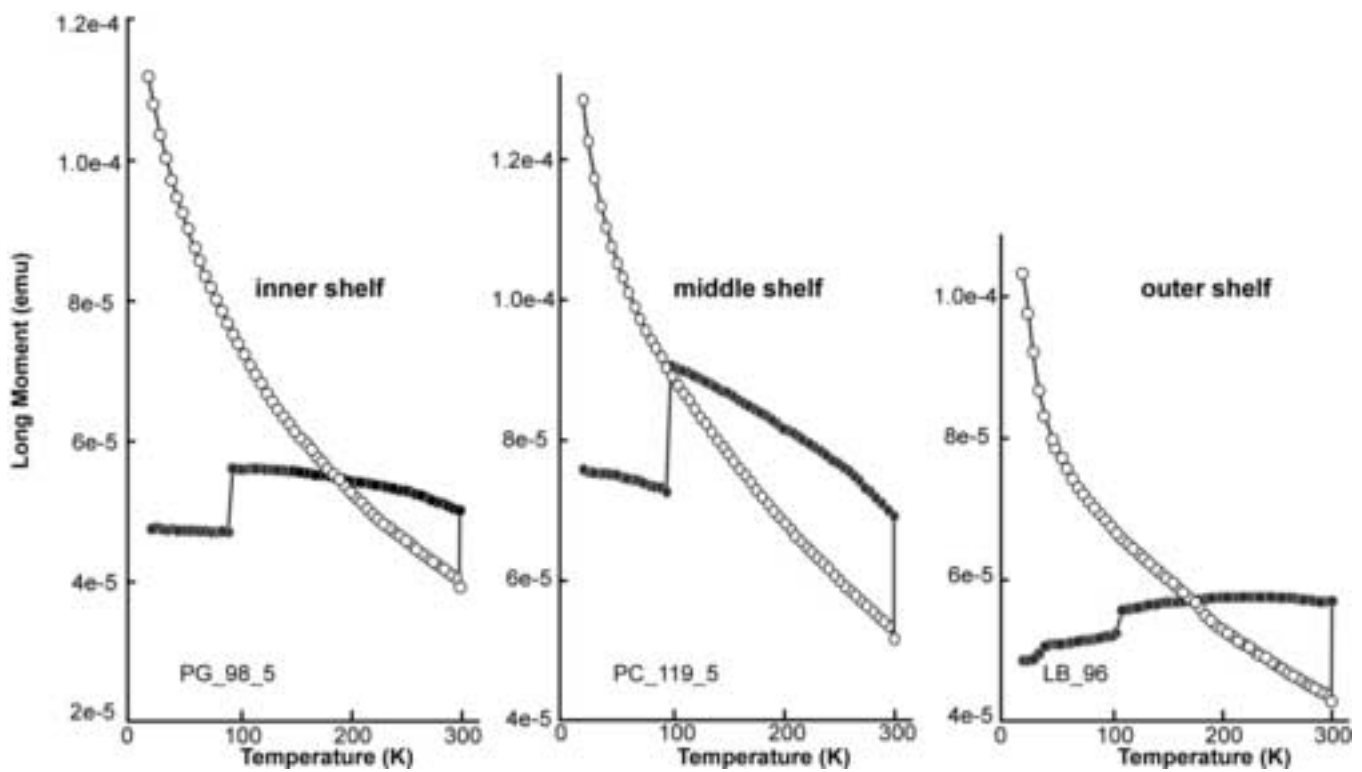


Figure 5  
[Click here to download high resolution image](#)

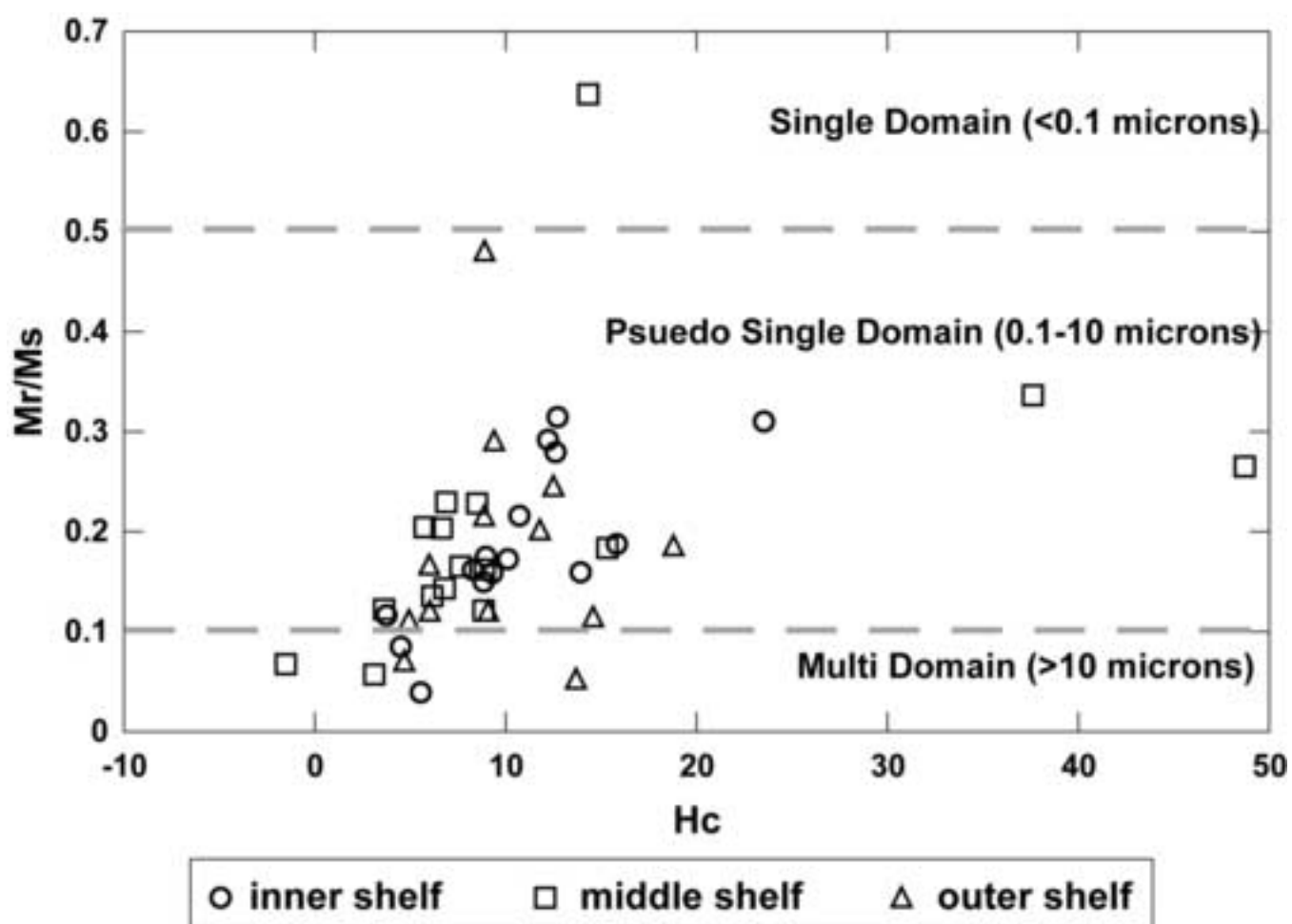


Figure 6  
[Click here to download high resolution image](#)

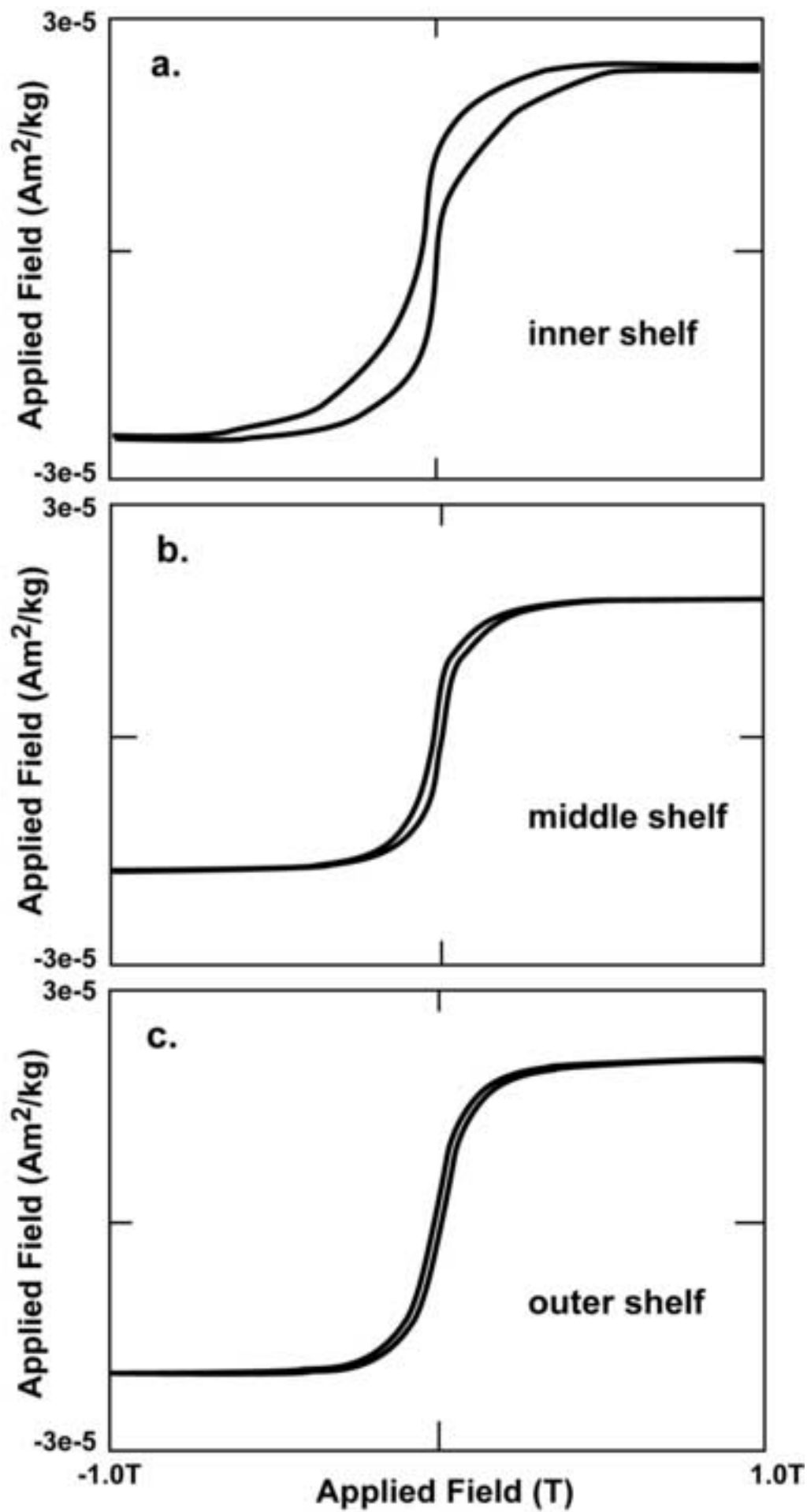


Figure 7  
[Click here to download high resolution image](#)

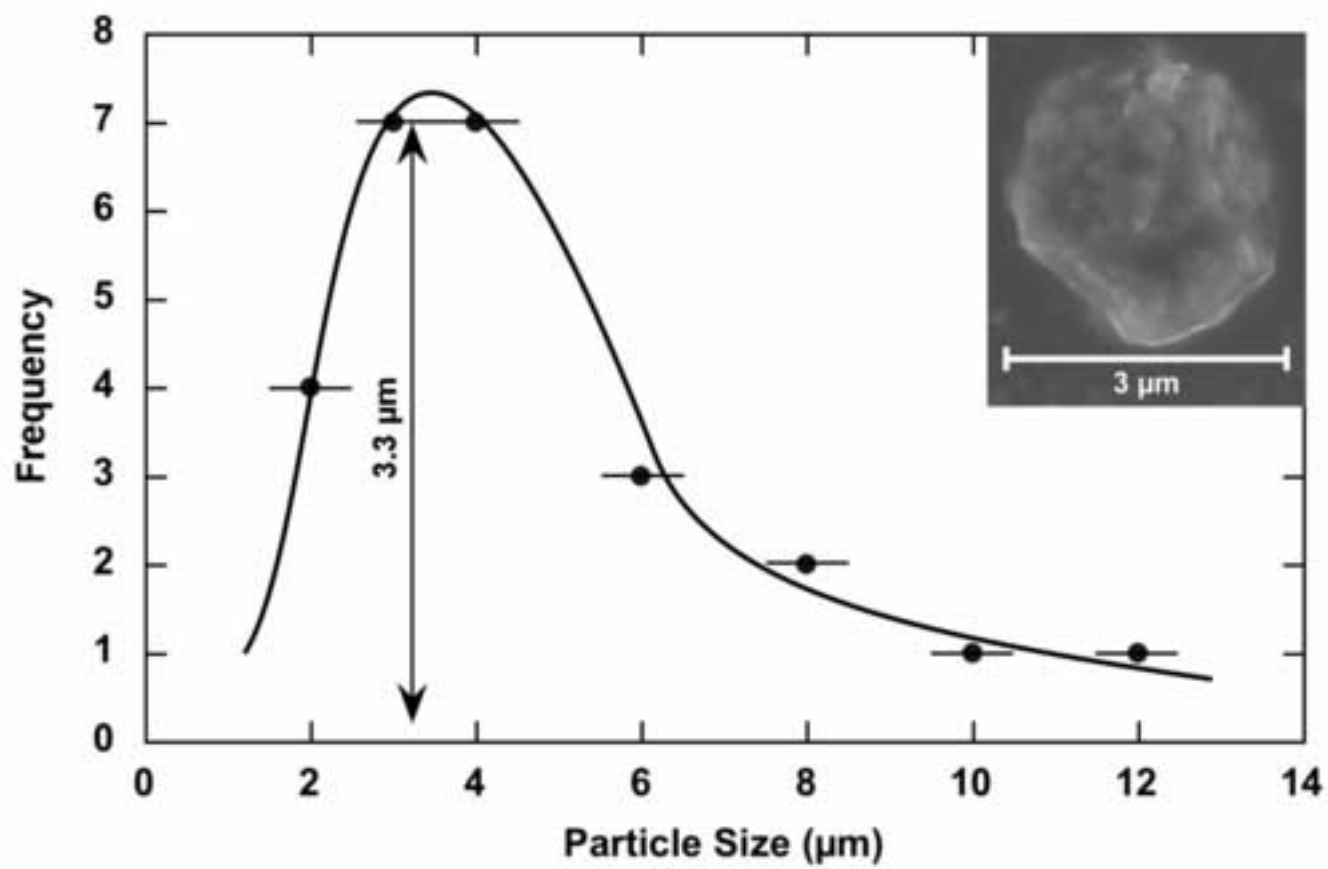




Figure 8  
[Click here to download high resolution image](#)

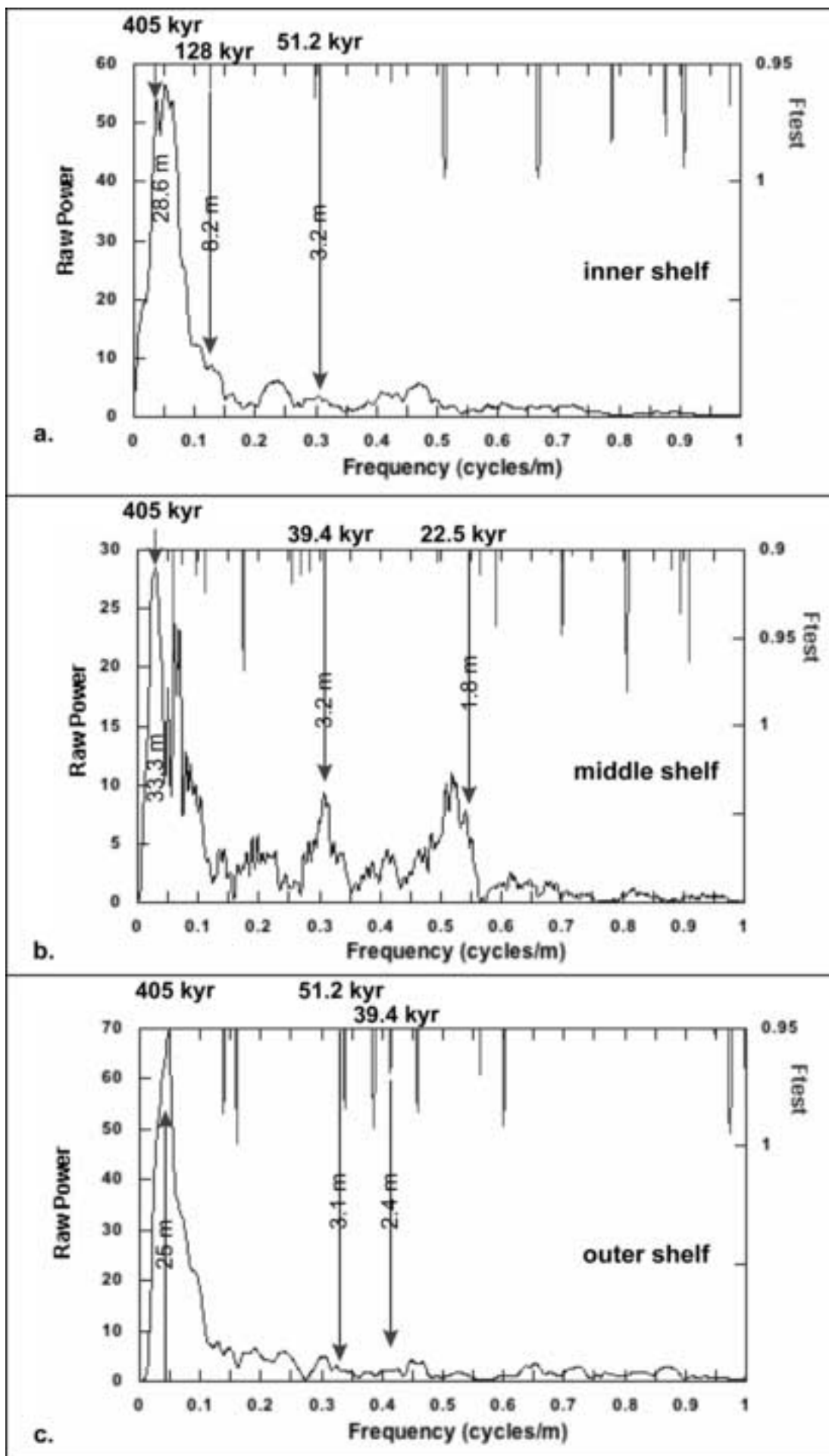


Figure 9  
[Click here to download high resolution image](#)

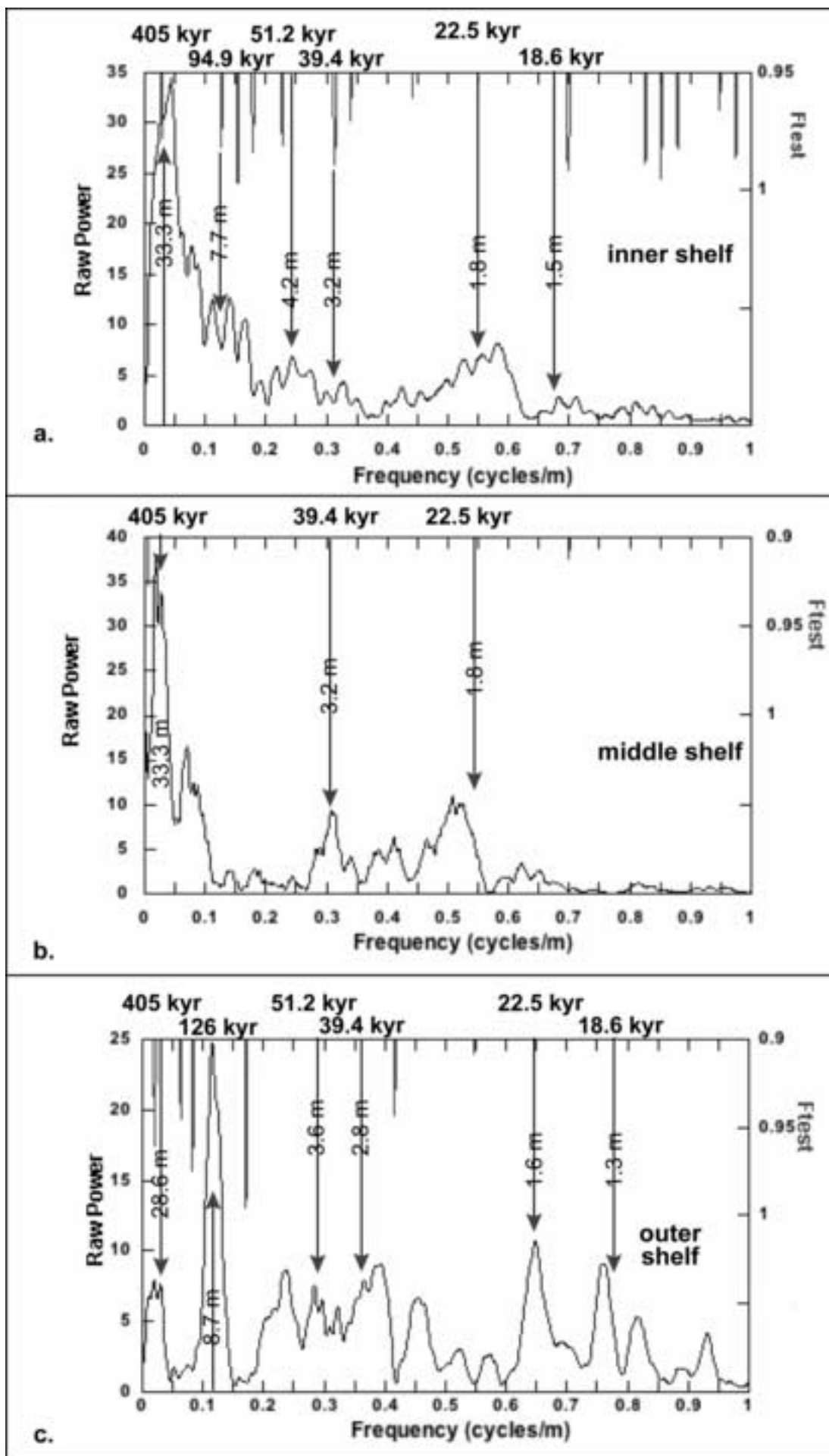


Figure 10  
[Click here to download high resolution image](#)

